A Comparison of Atlantic, Pacific and Instant Ocean^{TM} Seawaters using Palmitic Acid and

Hexadecanol Monolayers as Model Atmospheric Films

Undergraduate Research Thesis

Presented in Partial Fulfillment of the Requirements for graduation "with Honors Research

Distinction in Chemistry" in the undergraduate colleges of The Ohio State University

by

Evan A. Lach

The Ohio State University

May 2018

Project Advisor: Professor Heather C. Allen, Department of Chemistry & Biochemistry

Committee Members:

Dr. Rafael Jimenez-Flores, Department of Food Science and Technology

Dr. Noel M. Paul, Department of Chemistry & Biochemistry

Abstract

Sea spray aerosol (SSA) is a major factor in global climate change modeling but is still one of the most uncertain forcing factors. Organic and ionic chemical species within SSA account for only some of the complexity, but can alter properties of these aerosols that affect their interaction with atmospheric systems. **Palmitic acid (PA)** is found in SSA, originating from cellular membranes in the **sea surface microlayer (SSML)**. **Hexadecanol (Hex)** is an efficient ice nucleator and is found in the SSML, produced from biological activity. The importance of the SSML as a site for heterogeneous reaction and transfer of chemical species to SSA cannot be understated, so ongoing study is necessary. Since there are so many species in the SSML, creating an effective proxy for use in laboratory work is important to be able to isolate distinct chemical players. Within this thesis, the changes in the surface behavior of PA and Hex on pure water, Atlantic seawater, Pacific seawater, and **Instant Ocean (IO)** are compared using Langmuir **pressure-area (Π-A)** isotherms, **Brewster angle microscopy (BAM)**, and **infrared reflection-absorption spectroscopy (IRRAS)**.

On Atlantic and Pacific seawater relative to pure water, PA showed condensation at low **surface pressure (Π)** (Δmean molecular area (MMA)) = 2-3 $Å^2$/molecule). As area decreased, there was a loss of phase change with increasing Π, monolayer expansion at high Π, leading to collapse at higher Π than on pure water. BAM images on these seawater subphases showed minimal aggregate formation after collapse in contrast with pure water. The PA monolayer was more compressible on real seawater than pure water. The C-H and carboxyl IRRAS modes changed depending on system pH and organics, and the PA monolayer packed hexagonally. These dynamics can be slated to a balance between expansion-inducing organics and

contraction-inducing pH and ionic effects from the seawaters. On these same subphases, Hex showed expansion relative to pure water throughout the isotherms with a retention of phase change on seawater. BAM images showed some aggregation on Pacific and Atlantic seawater, and the Hex monolayer was again more compressible than on pure water. Peaks in IRRAS were analyzed in the CH stretching and CH scissoring regions, showing similar organic content and hexagonal packing on the real seawater subphases. Hex interacted less strongly with the subphases than PA, as expected because of the alcohol headgroup on Hex that maintained neutrality regardless of system pH.

On IO, PA and Hex were greatly expanded and showed 3D aggregation earlier that remained throughout compression. Both lipids were most compressible on IO out of any subphase, meaning the surfaces could change their packing efficiently to offer the least resistance to compression. For PA on IO, IRRAS results were irreproducible, which is likely due to interfacial aggregation even at low Π. For Hex, IRRAS results were also variable, but less so than PA, again showing the tendency of PA to interact with the subphase more strongly. Based on these results, IO does not work as a proxy for real seawater in our lab. Alternatively, a house-made **artificial seawater (ASW)** matched real seawater data best based on preliminary trials, but was hard to maintain within desired specifications. In the future, the ASW should be explored further for seawater study in our lab. After a suitable proxy has been determined, the fundamental chemical interactions in the SSML that influence global climate can be probed in even more representative systems in the lab.

Dedication

I dedicate this thesis to my parents, Brian and Susan Lach who have taught me to finish what I start and have encouraged me throughout every pursuit.

Acknowledgments

I would like to thank the Allen group members for their individual contributions to my scientific development, whether through discussions on data or in passing conversation. I thank Dr. Allen for her support, teaching, and excitement throughout these four years in her group. Finally and most greatly, I thank Bethany Rudd-Wellen, my graduate advisor, for being ever present during my research experience to offer guidance and help with any issue (even when I had to schedule research time at 8am). Her mentorship has helped me beyond measure in developing analytical skills, from lab practice to data analysis and communication.

Publications

Wellen, B. A.; Lach, E. A.; Allen, H. C. Surface pKa of octanoic, nonanoic, and decanoic fatty acids at the air-water interface: applications to atmospheric aerosol chemistry. *Phys. Chem. Chem. Phys.* **2017***, 19*, 26551-26558.

Table of Contents

Table of Figures

Table of Abbreviations and Symbols

Abbreviations

ASW	Artificial Seawater
BAM	Brewster angle microscopy
Hex	Hexadecanol
IO	Instant Ocean^{TM}
IRRAS	Infrared Reflection-Absorption Spectroscopy
MM	Molar mass
MMA	Mean Molecular Area
PA	Palmitic Acid
RA	Reflectance-Absorbance
RH	Relative Humidity
SSA	Sea Spray Aerosol
SSML	Sea Surface Microlayer
TC	Tilted Condensed
UC	Untilted Condensed

Symbols

A	Area
Å	Angstrom
C^{-1}	Compressibility Modulus
cm^{-1}	Wavenumber
E_s or E_p	*s*- or *p*-polarized Electric Field Vector
mM	Millimolar
mN/m	milliNewtons per Meter
N_A	Avogadro's Number
γ	Surface Tension
Π	Surface Pressure

Chapter 1: Introduction

1.1 Atmospheric Relevance

The surface of water is an interface that hosts chemical and physical interactions unique from the bulk. Certain molecules called surfactants lower the free energy of the interfacial system when partitioned to the surface rather than the bulk of the solution due to their hydrophilic properties.[1] The amphiphilic nature of surfactants heterogeneously exposes them to gas and liquid phases.[2] These surfactants are held on the water surface rather than released into the gas phase through hydrophilic interactions with their polar functional groups proximal to their hydrophobic portions. In nature, films of organic molecules form on the surfaces of bodies of water, including the oceans. The layer situated at the top few micrometers of the oceans is termed the sea surface microlayer (SSML) and is a dynamic feature, being perturbed by mechanical processes then reforming.[3] Perturbation of this layer via wave breaking can cause ions and organics to be promoted from the SSML to the atmosphere on aerosol particles through film and jet drops[4,5] to create sea spray aerosol (SSA). Atmospheric aerosols have the largest uncertainty of global climate forcings,[6] and the organic coatings on these particles are highly influential on global climate.[7] Aerosols can scatter solar radiation[8] and act as cloud condensation nuclei,[9] which are both negative temperature forcings. Secondary effects from higher cloud coverage can be positive temperature forcings, due to processes such as greenhouse gas trapping and absorption of solar radiation.[10] To consider specific chemical players, fatty acids and alcohols are a subset of molecules present in the SSML. The hydrocarbon chains are oriented towards the gas phase and the hydrophilic head groups (-COOH or –OH specifically) are pointing into the water surface.[11] **Palmitic acid (PA)** is a C_{16} saturated carboxylic acid with a

relatively enhanced presence in SSA,[12,13] and **hexadecanol (Hex)** is the C_{16} alcohol analogue to PA; both of these molecules are shown in Figure 1.

palmitic acid
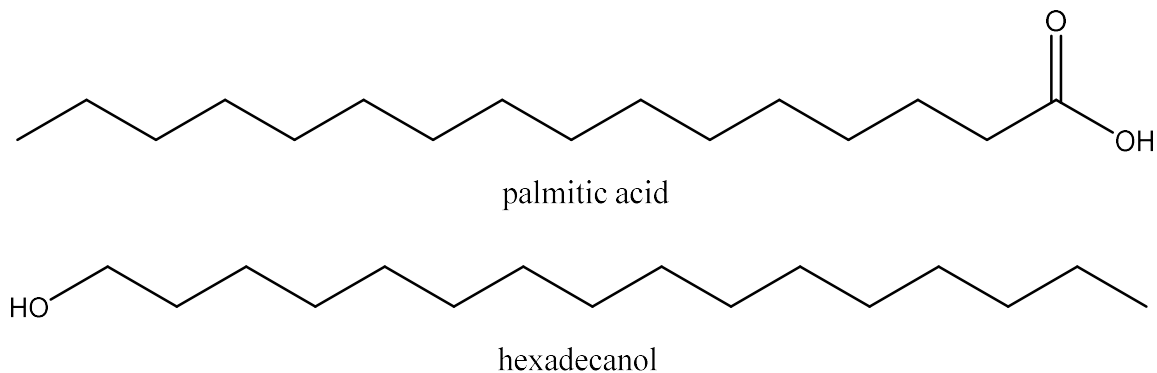
hexadecanol

Figure 1: Molecular structures of palmitic acid and hexadecanol.

PA is commonly used as a proxy for the fatty-acid content of oceanic aerosols,[14] while hex is generated from bacteria in atmospheric aerosol particles,[15,16] and acts as an efficient ice nucleator.[17,18] The environment around these molecules affects their surface behavior, and the interactions of these specific molecules with different seawater environments are studied within this thesis. The big-picture goals is to apply insight from fundamental lab study to these same molecules in complex, climate-altering SSA environments.

1.2 Subphase Effects on Interfacial Species

As this research focuses on the surface of water, it is worth considering what effects the bulk of a liquid can have on the surface. The presence and function of ions at the surface of water is a topic under debate in the literature.[19,20,21] Traditionally, ions were thought to be repelled from the surface due to the observed increase of surface tension of aqueous salt solutions,[22] but this fails to acknowledge the distinct behavior of cations and anions at the interface.[23] There is now data to suggest the importance of cations and anions in interfacial phenomena, from their

involvement in heterogeneous reactions[24] to the physical alteration of atmospherically relevant monolayers.[14] Organic surfactants can interact with ions in the interfacial region through their polar head groups. Spectroscopic studies of the interactions between PA and Mg^{2+} or Ca^{2+} showed alteration of surface ordering, and even metal-induced deprotonation of the -COOH group.[25,26] Divalent ions typically interact more strongly with carboxylic acids due to their higher charge density, however, altered monolayer ordering effects have also been seen for monovalent Na^+.[14] These surface-ion effects can change how organics are transferred into SSA: the presence of ionic species has been shown to correlate with greater uptake of surfactant organics onto SSA.[27]

Along with ions, the pH of the bulk solution can have a great effect on the surface. For a given solution, the ionization state of a surfactant at the interface is not necessarily the same as in the bulk,[28] so pH effects are another variable to control in fundamental atmospheric experiments. Van der Waals interactions between hydrophobic tails pack PA close together at the surface, bringing the carboxyl headgroups closer together.[28,29] This increases the energy barrier to deprotonation and thus increases the pK_a at the interface: PA has a bulk pK_a near 5 and an interfacial pK_a of 8-9.[29] With an ionizable carboxyl- head group, PA is sensitive to pH change in aqueous media, and its monolayer undergoes organizational change as bulk pH is increased and deprotonation is induced.[14] Deprotonated acids have a charge and become more soluble as the fraction of ionized species increases, so the pH also affects the efficiency of surface coverage. Oceanic pH is near 8.1,[30] and varies per geographical location, so the PA molecules are expected to be at least partially deprotonated in oceanic conditions. The surface ionization state is a hot topic in the literature, and has mainly been explored for organic acids. Hex is less affected by pH

because its hydroxyl headgroup has a pK_a near 15 and is appreciably unaffected by a subphase pH of 8. Any changes of its ionization behavior at the interface have not yet been explored.

The ocean not only has a mixture of ionic salts and a basic pH, but also has organic matter that varies with location and time; the complexity of seawater as a subphase for interfacial study makes it a difficult target. Specific species in real seawater include: cations (Na^+, K^+, Mg^{2+}, Ca^{2+}, Sr^{2+}); anions (Cl^-, SO_4^{2-}, CO_2 speciation); nutrients (phosphates, nitrates, ammonium, Si-O species, dissolved organic phosphate, dissolved organic nitrogen, dissolved organic carbon); and trace element speciation (Li, Si, Mo, Ba, V, Ni, Cr, Al, Cu, Zn, Mn, Fe, Cd, Pb, Co, Ag, Ti).[31] By creating proxy systems in the lab that mimic atmospheric environments, we can isolate the effects of individual components within the environment, and the complexity of atmospheric systems can be reduced to better understand discrete effects. Although there are commercial products available that mimic the composition of the ocean, the purity of these may not be adequate for use within a surface-science laboratory. As an alternative to commercial products, a house-made seawater proxy could be formulated. By creating an artificial mixture accounting for only the major salts and pH (Na^+, Mg^{2+}, Ca^{2+}), the complexity can still be decreased for laboratory analysis. Even so, the manner of interaction is far from trivial because of the combination of mono- and divalent ions creates a high ionic strength environment that alters surfactant modes of interaction. In this thesis, the surface behaviors of PA and Hex on Atlantic seawater, Pacific seawater, and Instant Ocean^{TM} are contrasted to that on pure water to evaluate an appropriate subphase for oceanic surface study in the lab. With an appropriate proxy, fundamental interactions probed in the lab will lead to a decrease in the uncertainty associated with SSA in the climate.

Chapter 2: Theory and Instrumentation

2.1 Surface Tensiometry

2.1.1 Surface Tension

One of the most common physical methods to study surface packing is surface tensiometry. **Surface tension (γ)** is the two-dimensional cohesive force between liquid molecules at the liquid-gas interface.[11] It acts to minimize the surface area of liquids and is the reason water droplets form as spheres.[32]
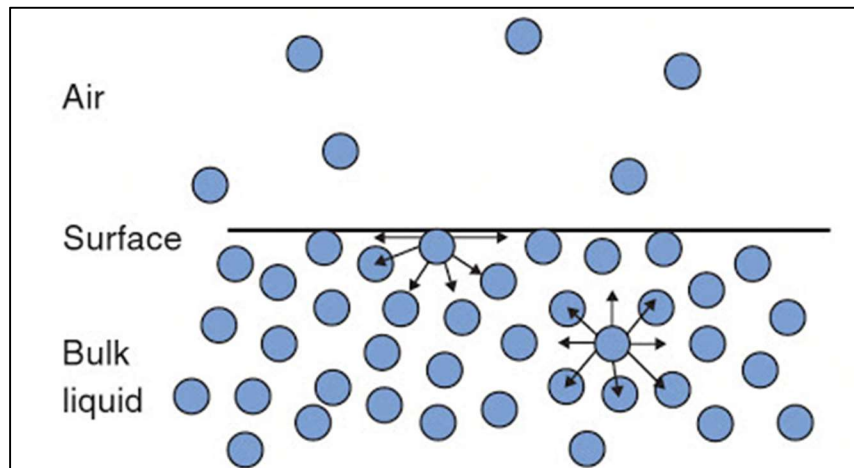
Figure 2: A graphical represenation of forces involved in surface tension, taken from [32] pg. 12, showing forces as vectors on molecules represented as spheres.

As shown in the figure taken from [32], lateral intermolecular force components at the surface cancel, leaving force vectors pointed towards the bulk of the liquid. Surface tension can be defined considering the force F tangent to the surface, acting normal to an element δx as:[32]

$$\gamma = \frac{F}{\delta x} \qquad\qquad 2.1$$

On water, hydrogen bonding and dipolar interactions dominate this force that acts inward. When there is a surfactant layer on top of a water subphase, the cohesion between water molecules is disrupted, leading to a decrease in surface tension from the pure water value of 72.1 mN/m.[11] Therefore, surface tension techniques are a useful way to study surfactant monolayers on water. The γ of a system can be experimentally probed with a Wilhelmy plate, shown in Figure 3.
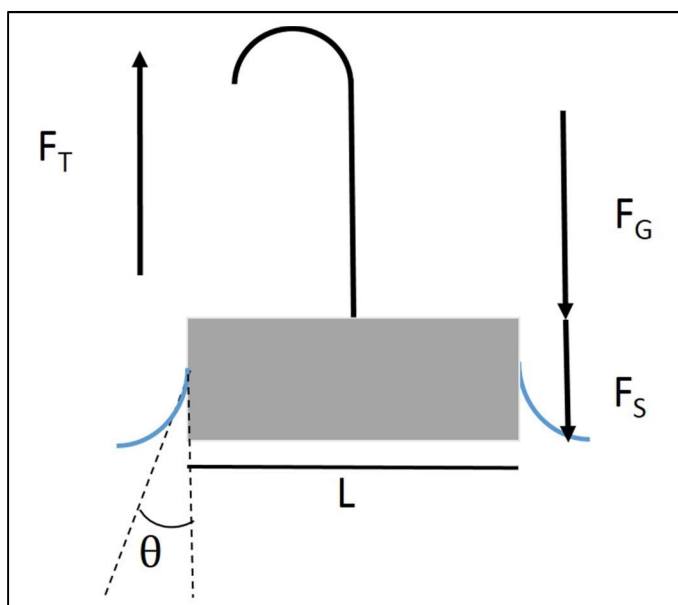
Figure 3: A Wilhelmy plate with interfacial forces, contact angle, and plate length shown.

The Wilhelmy plate relates to surface tension through:[32]

$$\gamma = \frac{F}{2(L + y)cos\theta} \qquad\qquad 2.2$$

where F is the force on the plate, L is its length and y is its thickness. The buoyancy is negligible when the bottom edge of the plate is level with the liquid surface. This relationship can be simplified by reasonably assuming the contact angle between water and the plate to be 0° for a completely wetted plate, yielding:

$$\gamma = \frac{F}{2(L + y)} \qquad\qquad 2.3$$

2.1.2 Surface Pressure

Surface **pressure (Π)** is defined as the difference in surface tension between pure water (72.1 mN/m) and water covered with a surfactant:

$$\Pi = \gamma_{pure} - \gamma_{surfactant}$$

As surface coverage increases, the Π increases in response to the decrease in $\gamma_{surfactant}$.

2.1.3 Langmuir Isotherms[11]

A Langmuir isotherm experiment allows us to study the dynamics of Π as a monolayer is compressed. A hydrophobic trough of known area is filled with water or aqueous subphase, then a surfactant in a volatile solvent is spread onto the water surface via droplets from a syringe. After allowing the solvent to evaporate, mobile barriers reduce the area available to the monolayer over time, forcing the molecules to pack together more tightly. Results can be plotted as Π versus **mean molecular area (MMA)**, which is a quantity describing the average area each molecule occupies within the monolayer. These experiments are therefore referred to as Π-A isotherms. MMA can be calculated via:

$$MMA = \frac{A}{cN_A V} \qquad\qquad 2.4$$

where A is the area available to the monolayer, c is the molar concentration of the solution spread on the interface, N_A is Avogadro's number, and V is the volume spread onto the surface.

By controlling compression, the monolayer reorganizes to exist in different phases depending on the area available to the molecules. These Π-A plots are read right-to-left as plotted in this thesis since the MMA is decreased in the experiment. Figure 4 (modeled from [33]) is an example of a Π-A isotherm that illustrates the different phases accessible to fatty acids and alcohols. The monolayer starts in a phase with minimal intermolecular interactions, passes the "liftoff point" at (a), goes through the liquid condensed with some tighter packing, then finally to the solid phase in which a sheet covering the water surface is formed indicated by a change in slope at (b). At point (c), the monolayer "collapses" and three-dimensional aggregate structures can be formed as surfactant molecules buckle on top of one another since the MMA is too small for each molecule to favorably occupy a discrete space on the surface.
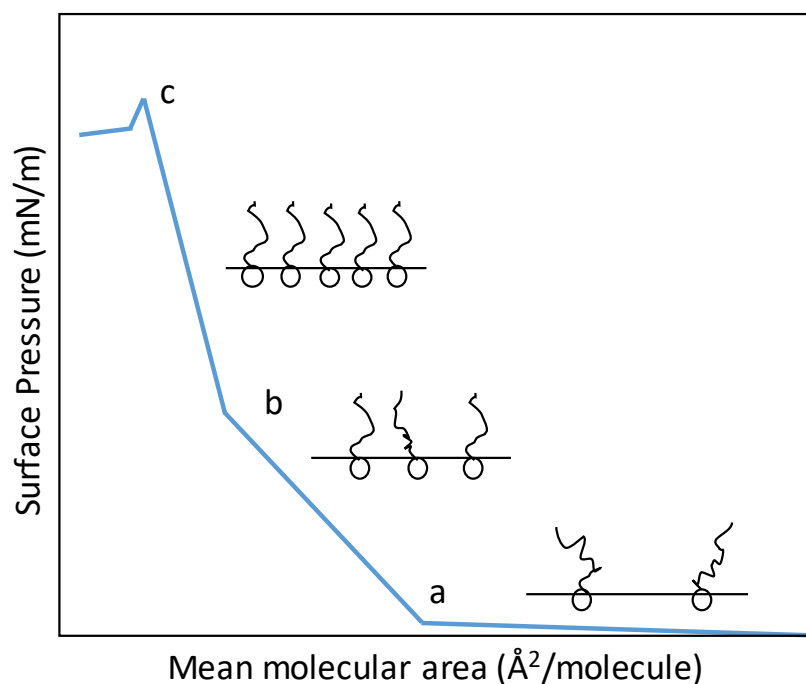
Figure 4: The example output of a Langmuir Π-A isotherm experiment (modeled from [33]) showing cartoon molecular interactions at various MMA and Π values. (a) is the gas-liquid condensed phase, (b) is a liquid untilted-condensed phase, and (c) is a liquid tilted-condensed phase.

The surface pressure at collapse (point (c)) is indicative of monolayer stability at low MMA. A

higher collapse pressure indicates a more stable metastable state prior to collapse. The structure of the isotherm past collapse (past point (c)) indicates how surfactant molecules behave after collapse: if more negatively sloped, molecules are departing from the monolayer faster than if this region has less slope, whether this is through desorption or 3D aggregate formation.

The changes in PA and Hex isotherm characteristics on seawater relative to pure water enable conclusions about their surface behavior. In general, increased organic presence in the subphase (especially surface-active organics) causes the monolayer to expand, meaning MMA values would be shifted higher. Salts and pH can have multiple effects on surface-active species, as discussed in the introduction. The balance of interactions between expanding and contracting effects on the monolayer are shown in isotherm data in this thesis.

2.1.4   Compressibility Modulus[11]

Π-A isotherm data may be analyzed to yield the compressibility, C, of a monolayer:

$$C = -\frac{1}{MMA} * \left(\frac{\delta MMA}{\delta \Pi}\right)_{T,P,n_i} \qquad 2.5$$

using MMA values and changes in MMA over changes in Π. This is the interfacial analogue of the bulk compressibility of a material. By taking the reciprocal of this quantity, the compressibility modulus, C^{-1} is obtained.[34]

$$C^{-1} = -MMA * \left(\frac{\delta \Pi}{\delta A}\right)_{T,P,n_i} \qquad 2.6$$

This quantity is more directly useful since the change in Π over the change in MMA is simply the derivative of the Π-A isotherm data. Comparison of C^{-1} values for a lipid in different systems shows how the compressibility of that lipid changes in response to that system. Higher values of

C[-1] indicate a more rigid monolayer that is *less compressible*. For example, a monolayer in the gaseous phase would be more compressible and have a lower C[-1] value than a monolayer in a condensed phase since there is more area available to a monolayer in the gas phase.

2.2 Brewster Angle Microscopy[35]

There are ways to image the surface of water when covered with surfactant molecules, one of them being **Brewster angle microscopy (BAM)**. The Brewster angle (θ_B) is measured from the surface normal, is a property specific to each interface, and is the angle at which there is no reflection of *p*-polarized light.
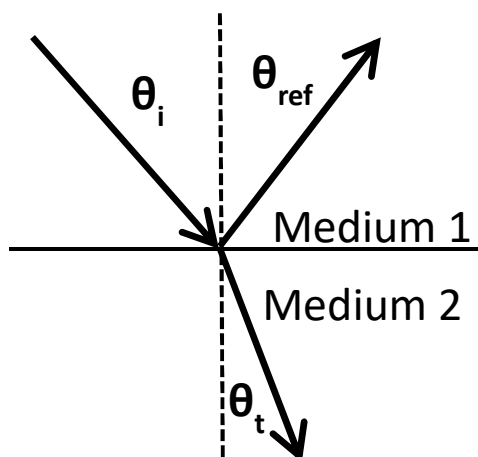
Figure 5: The interaction of light with an interface showing the angle of incidence (θ_i), angle of reflection (θ_{ref}), and angle of refraction (θ_t), all relative to the surface normal

The Brewster angle for pure water, 53.1°, can be derived by considering the Fresnel equations for *s*- and *p*-polarized light:

$$R_s = -\frac{sin(\theta_i - \theta_t)}{sin(\theta_i + \theta_t)} \qquad 2.7$$

$$R_p = -\frac{tan(\theta_i - \theta_t)}{tan(\theta_i + \theta_t)} \qquad 2.8$$

From equation 2.8, The reflectivity of p-polarized light tends towards zero as $\theta_i + \theta_t$ approaches 90°. Using this condition within Snell's law of refraction between materials of different refractive indices, the Brewster angle can be calculated.

$$n_1 \sin(\theta_i) = n_2 \sin(\theta_t) \qquad\qquad 2.9$$

$$\frac{n_1}{n_2} = \frac{\sin(\theta_t)}{\sin(\theta_i)} = \frac{\sin(\theta_t)}{\sin(90° - \theta_t)} = \frac{\sin(\theta_t)}{\cos(\theta_t)} = \tan(\theta_t) \qquad\qquad 2.10$$

$$\theta_B = 90° - \arctan\left(\frac{n_1}{n_2}\right) = \arctan\left(\frac{n_2}{n_1}\right) \qquad\qquad 2.11$$

So, the ideal Brewster angle can be obtained using just the **refractive indices (n_i)** of air (1.000) and water (1.333) in this case.

This property proves useful to separate signals from the water and from the monolayer using p-polarized light since n_{water} is different from $n_{surfactant}$. As such, using the Brewster angle for pure water allows us to image the monolayer with bright areas in the image indicating surfactant coverage and dark areas indicating lack of surfactant. Rather than just obtaining an image of a monolayer in a steady state, this technique is combined with a Langmuir isotherm and continual imaging to obtain surface morphology at multiple Π or MMA values.

2.3 Infrared Reflection-Absorption Spectroscopy[35]

In addition to microscopy, spectroscopy can yield orientational information within the monolayer. IR radiation can be introduced to the interface by using mirrors to direct a beam onto a water surface. If the incident light has energy closely matching the vibrational energy gaps between monolayer species, it can be absorbed as it is reflected, leading to a reflected beam of

light carrying the vibrational information of the monolayer. The depth probed by IRRAS is debated, and the surface sensitivity comes from the mean free path of interaction of the IR beam at the surface. The intensity of absorption of infrared radiation is proportional to the square of the electric field vector, and the incidence angle of 46° to the surface normal yields optimal signal.[36] The **reflectance-absorbance (RA)** unit is the result of a logarithmic division of sample (R) and reference spectra (R_o):

$$RA = -\log\left(\frac{R}{R_o}\right) \qquad 2.12$$

For example, a spectra for PA on pure water is the result of the above calculation from a spectrum taken of pure water and one taken with PA on the surface at the select surface pressure. The peaks of interest in the spectra shown are those with negative RA values because of the unpolarized light from the instrument.

Chapter 3: Materials and Methods

3.1 Materials

All lipids were used without further purification: 99% palmitic acid, and 99% 1-hexadecanol were purchased from Sigma Aldrich (St. Louis, MO). HPLC grade chloroform and ACS grade > 99% NaCl, $MgCl_2$, and $CaCl_2$ were purchased from Fisher Scientific. PA was prepared to 2.1 mM, and Hex to 4.5 mM each in chloroform and were stored in a dark freezer when not in use. The NaCl was baked before use for 6 hrs at 600 °C, while stock solutions of $MgCl_2$ and $CaCl_2$ were filtered three times through Whatman Carbon-Cap 75 activated carbon filters (Fisher Scientific) before standardization via Mohr titration. Pellets of 99% NaOH were purchased from Mallinckrodt (Paris, KY). Ultrapure water from a Millipore Advantage A-10 Milli-Q Integral

water purification system with resistivity 18.2 MΩ•cm and TOC < 5 ppb was used for all aqueous solutions and experiments other than those involving Instant Ocean™ (IO), which was prepared in tap water to maintain conformity with its package directions (see section 4.3.2 for concerns about purity). The Pacific Ocean seawater was obtained from The Scripps Institute pier in La Jolla, CA in December 2016. The Atlantic Ocean seawater was obtained from Ocean City, MD in July 2016. These samples were stored in a refrigerator at 2 °C and allowed to warm to ambient temperature before use. Nalgene plastic bottles that had been cleaned with Hellmanex detergent then rinsed 20 times with nanopure water were used for all seawater storage.

3.2 Methods

3.2.1   Solution Preparation

IO was prepared as directed on the packaging; for the scale used in these experiments, 35 g was dissolved in 1 L tap water. The concentrations of major species in IO are given in Table 1, as provided by the company for a 35 ppt solution salinity. The IO prepared following package directions has a salinity of ~32 ppt.

Ion	Instant Ocean (ppm)	Seawater (ppm)[37]
Cl^-	19,290	19,353
Na^+	10,780	10,781
SO_4^{2-}	2,660	2,712
Mg^{+2}	1,320	1,284
K^+	420	399
Ca^{+2}	400	412
CO_3^{2-} / HCO_3^-	200	126
Br^-	56	67
Sr^{2+}	8.8	7.9

Boron	5.6	4.5
F^-	1.0	1.28
Li^+	0.3	0.173
I^-	0.24	0.06
Ba^{2+}	less than 0.04	0.014
Iron	less than 0.04	less than 0.001
Manganese	less than 0.025	less than 0.001
Chromium	less than 0.015	less than 0.001
Cobalt	less than 0.015	less than 0.001
Copper	less than 0.015	less than 0.001
Nickel	less than 0.015	less than 0.001
Selenium	less than 0.015	less than 0.001
Vanadium	less than 0.015	less than 0.002
Zinc	less than 0.015	less than 0.001
Molybdenum	less than 0.01	0.01
Aluminum	less than 0.006	less than 0.001
Lead	less than 0.005	less than 0.001
Arsenic	less than 0.004	0.002
Cadmium	less than 0.002	less than 0.001
Nitrate	None	1.8
Phosphate	None	0.2

Table 1: The concentrations of major ions in IO (from the company) and in real seawater[37] in ppm.

3.2.2 Π-A Isotherms

All experiments (including isotherms, microscopy, and spectroscopy) were conducted at 22 ± 0.8 °C and a measured relative humidity 33 ± 6 %. Π-A compression was conducted with Delrin barriers on a Teflon trough with area 14878 mm^2 and width 86 mm. Experiments were conducted with a KSV (Finland) 1000 IUD balance and tensiometer head with a Wilhelmy plate

cut from filter paper (perimeter 20.8 mm). The apparatus for these experiments is shown in Figure 6. Prior to lipid introduction, the surface was ensured to be clean by compressing the barriers to their maximum value and verifying the Π reading did not rise over 0.2 mN/m. The lipid was then spread to an MMA ~20 Å^2/molecule greater than its liftoff point onto 140 mL of a subphase. After a 10 minute waiting period to allow solvent evaporation, the barriers were compressed at 5.0 mm/min per barrier to 55 mm while recording Π. The results of Π-A isotherm experiments are reported as Π (mN/m) versus MMA (Å^2/molecule), with each trace representing the average of at least three trials (except IO traces, which comprised of two trials) with the corresponding standard deviation of the trials as shading around the curve.
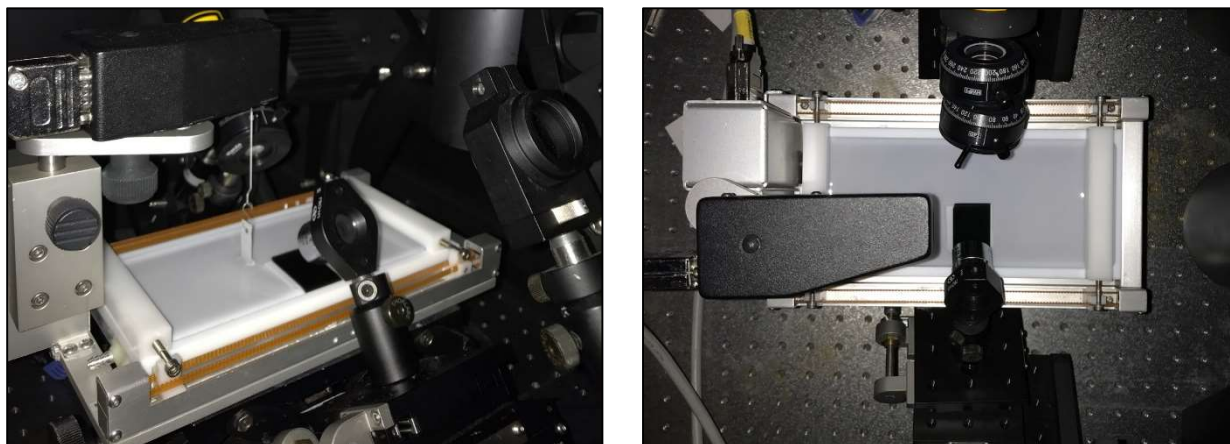
Figure 6: Left: Langmuir trough setup showing the Teflon trough and Delrin barriers, hanging Wilhelmy plate, and KSV balance. Right image: top view.

3.2.3   Brewster Angle Microscopy

As depicted in Figure 7, a Research Electro Optics (Boulder, CO) He-Ne laser (0.5 mW at 543 nm) impinged a half wave plate then a Glan polarizer before interacting with the subphase surface within the trough previously described. Refraction scattering was minimized with a density filter in the subphase. The beam then reflected off the surface, through a Nikon objective

lens (10X magnification/0.21 NA), then through a focal tube lens, and finally into an Andor iXON CCD paired with Andor SOLIS imaging software. Raw images were cropped to 400 x 400 μm to isolate interesting domains. Dark areas in images indicate no surface coverage, while lighter areas indicate surfactant coverage, and bright white areas indicate 3D surface domains. BAM results are labelled with the Π at which the image was taken and a 100 μm scale bar.
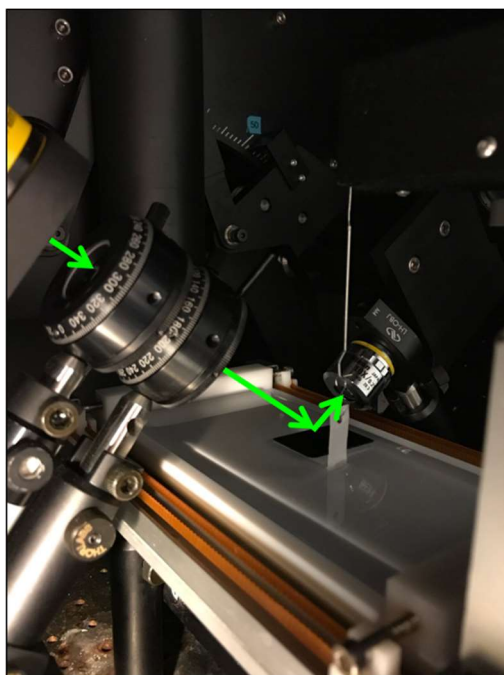
Figure 7: BAM setup showing the beam path with green arrows through the Glan polarizer, half wave plate, reflection off the surface, then objective lens.

3.2.4 IRRAS

A Perkin Elmer Spectrum 100 FTIR spectrometer was used for IRRAS collection in a custom-built enclosure seen in Figure 8. The incident IR beam hit a gold mirror to travel towards the surface at 46° to the surface normal, then reflected off the subphase surface to hit another gold mirror before reaching a liquid nitrogen cooled MCT detector. The scan range 4000-450 cm^{-1} was coaveraged over 300 scans with a resolution of 4 cm^{-1}. Spectra were then background subtracted in each of the regions of interest (ν(CH): 3000-2800 cm^{-1} and ν(C=O)/δ(CH): 1800-

1400 cm^{-1}) using the Peak Analysis tool in Origin 9 (Appendix 2: Peak Analysis in Origin), then three representative trials were averaged to yield the spectra presented here. For a single trial, PA was maintained at Π = 10 mN/m (the LC phase) throughout the acquisition time by allowing the barriers of the Langmuir trough to oscillate. For the rest of the trials, the PA was spread to an MMA corresponding to Π = 10 mN/m on each respective subphase in a petri dish of inner diameter 50 mm. Hex was spread to an MMA corresponding to Π = 5 mN/m (the LC phase) on the same size petri dish. There was no difference in spectral data whether or not the Langmuir trough was used to maintain Π. IRRAS results are plotted as RA versus IR wavenumber (cm^{-1}). The results from IRRAS on IO are plotted separately from the other subphases because of their irregularities.

Figure 8: The IRRAS setup housed in the PerkinElmer FTIR spectrometer with a Langmuir trough under the gold mirrors, with the IR beam path shown with red arrows.

Chapter 4: Results and Discussion

4.1 Palmitic acid

4.1.1   Π-A Isotherm

In general, the results from Atlantic and Pacific subphases are discussed relative to pure water first, then IO is compared to the other subphases separately. The Π-A isotherms of PA on pure water, Atlantic and Pacific seawaters, and IO are shown in Figure 9. On pure water, PA lifts off at 26 $Å^2$/molecule, has a phase change from liquid tilted condensed (TC) to liquid untilted condensed (UC) at 23 mN/m, then collapses abruptly at 38 ± 5 mN/m.[38] The liftoff point for PA is lower on both Atlantic (25 $Å^2$/molecule) and Pacific (24 $Å^2$/molecule) seawater subphases, showing a condensing effect at low Π. Additionally, the phase change at 23 mN/m on pure water is lost in the real seawater samples, which remain in a condensed phase throughout compression. The expanding effect of organics in the seawater is outweighed by a condensing effect at low Π. The condensation through some of the Π increase comes from the combination of pH and ionic effects. The pH of seawater is high enough to cause at least partial deprotonation of PA, and the charge formed on the carboxyl headgroup combined with ions like Na^+, Mg^{2+}, Ca^{2+}, etc. could create an environment for more efficient surface coverage. As alluded to earlier, the shielding of negative charge repulsions through metal binding allows closer packing of the surfactant molecules. Additionally, acid-soap complexes are known to form between ions and partially deprotonated surfactant acids to decrease surface tension efficiently[28,29] and tighten packing between molecules more than without the acid-soap complexes. A more tightly packed surface would be condensed, as seen in the isotherm. At Π = 15 mN/m on Atlantic and Π = 19 mN/m on Pacific, the isotherms show expansion versus on pure water. At the low MMA values

corresponding to these surface pressures, the organics in the seawater must outweigh the condensation from ions and pH, causing expansion. Near 35 mN/m on Atlantic and 40 mN/m on Pacific, there is a change in slope that indicates the organic species are being "squeezed out" of the monolayer as MMA is decreased further.

The pure water-PA system abruptly collapses around 38 mN/m and reorganizes to a state below 30 mN/m, while the Pacific system turns over around 45 mN/m and Atlantic has a more somewhat abrupt collapse around 40 mN/m. The increase in collapse pressure on seawater indicates greater metastability of the Atlantic and Pacific systems near collapse. This effect can be explained by ion presence: a PA molecule at the surface complexed to an ion is able to remain at the surface longer as the area is decreased because the ion enables tighter packing. The complex requires less area than a PA molecule alone, allowing the surfactant to pack tighter at the surface before collapse, which causes an increased Π prior to collapse. While PA at high pH without ions becomes more disordered at the interface and desorbs into bulk solution, with the addition of NaCl, PA has enhanced stability at the interface.[14] With the high ionic strength environment of the seawaters, the even greater stability at the interface observed here is not unreasonable. The "turn over" to collapse on Pacific could mean greater ionic impact at high Π to "ease" PA molecules into collapse packing, while the "somewhat abrupt" collapse on Atlantic could indicate greater organic impact at high Π that causes a sudden drop in Π due to crowding. The shapes of each seawater post-collapse are an artifact of averaging dissimilar post-collapse traces and would take further study to conclusively interpret. A final feature of these systems in Figure 9 is the wide span of the standard deviation in the real seawater subphases, which is discussed in section 4.1.4 below.

PA on IO is far expanded compared to any subphase, giving the first indication of the effects of IO contents on PA monolayers. A "true" liftoff point could not be determined for this system, as discussed in section 4.3.2, but by spreading the same amount of PA on the surface as the other systems in Figure 9, the isotherm lifted off at 42.5 $Å^2$/molecule. The pH was 8.2, so PA molecules were partially deprotonated and could potentially be brought closer via ionic-carboxylate charge interactions as in the seawater samples, but this was not observed. The organics in IO must overwhelm the condensing ability of ions and cause this great monolayer expansion. There are some similarities between IO and real seawaters relative to pure water: there is a lack of phase change in the isotherm and the monolayer reaches higher Π prior to collapse. However, IO has a more gradual slope throughout compression and reaches an even higher Π before collapse than the real seawater samples, indicating the monolayer that can reorganize well to accommodate surface packing at high Π. Additionally, the isotherm first turns over around 45 mN/m, but then slopes upward sharply at 50 mN/m before collapsing more abruptly at 57 mN/m. This turnover region between 25 $Å^2$/molecule and 18 $Å^2$/molecule is a metastable organization of the molecules on the surface, and the slope to a more abrupt collapse occurs when the MMA becomes too small for this metastable state. Notably, there is no indication of organic "squeeze out" on IO, meaning the organic content is well integrated with the PA on the surface.
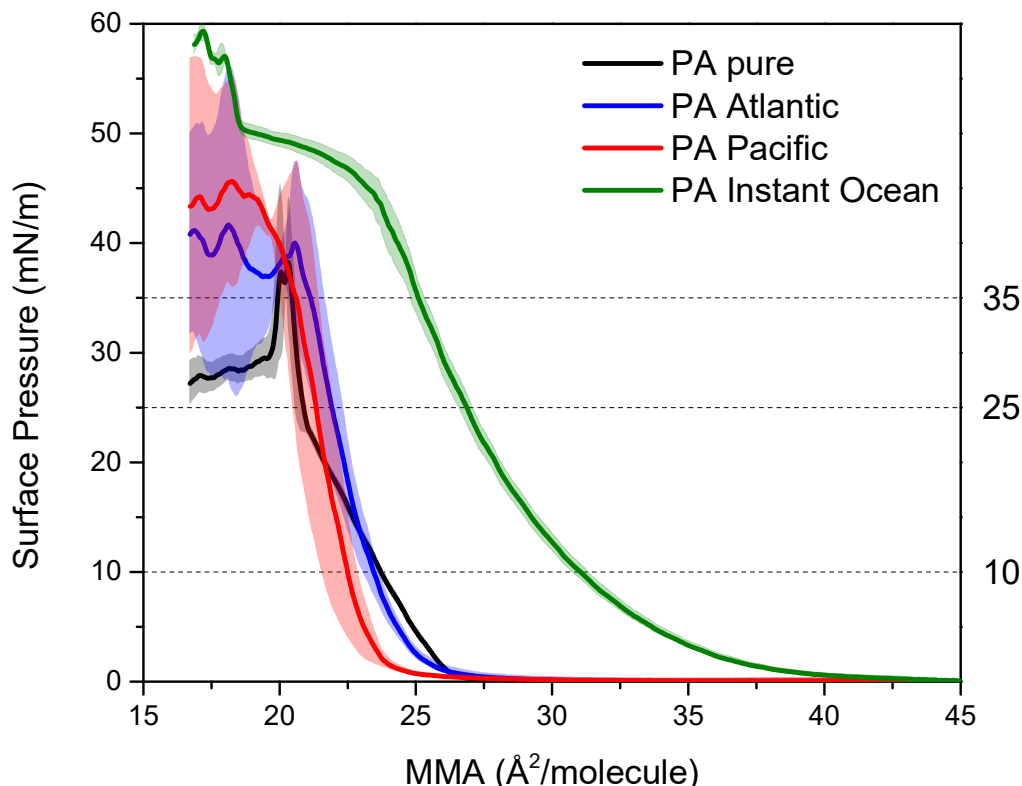
Figure 9: Π-A isotherms of PA on pure water, Atlantic, and Pacific seawaters, and IO with horizontal lines indicating Π values at which BAM images were taken.

4.1.2 BAM

The BAM images in Figure 10 are complementary to the isotherms of PA on each subphase. The condensing effect of the seawater samples is shown from the first images at 0 mN/m: on pure water PA forms circular domains while on Atlantic or Pacific seawater there are no circular domains and a sheet is already formed. Moving to the images in the 10-35 mN/m range, there is not much difference in domains between the pure water and real seawater subphases: each shows a sheet covering the full area starting at 25 mN/m. However, the seawater images are brighter than the pure water images, meaning the laser is reflected more efficiently, indicating tighter packing, in agreement with the isotherm data. The collapse images are also telling: on pure water the 3D aggregates PA is known to form[38] are shown as bright white shapes

in Figure 10. There is only one 3D-type structure in the Atlantic image, and no structures observed in the Pacific system, which again points to monolayer stability. Aggregates form on pure water because it is more energetically favorable for PA to stack on itself rather than desorb into the bulk. On seawater, the monolayer aggregates less as it collapses, meaning it is more energetically favorable for the monolayer to remain and reorganize as a monolayer than for aggregation to occur. These BAM images are visual evidence to suggest the isotherm data was interpreted correctly.

The BAM images of PA on IO agree with the high organic crowding observed from the isotherms: at 0 mN/m, there are organic signatures present that do not look like PA on any other subphase. While not shown here, even before PA was introduced, there were domains observed on the surface, indicative of the surfactant contamination within IO. At 0 mN/m, the domains do not resemble any of the other subphases. At 10 mN/m, small circular 3D aggregates are already formed, and these increase in presence at the surface through the rest of the compression. In the bottom image of column (d) in Figure 10, there are many, small 3D aggregates present that do not resemble those obtained on pure or real seawater, showing the divergence of IO from real seawater for these surface-study applications.
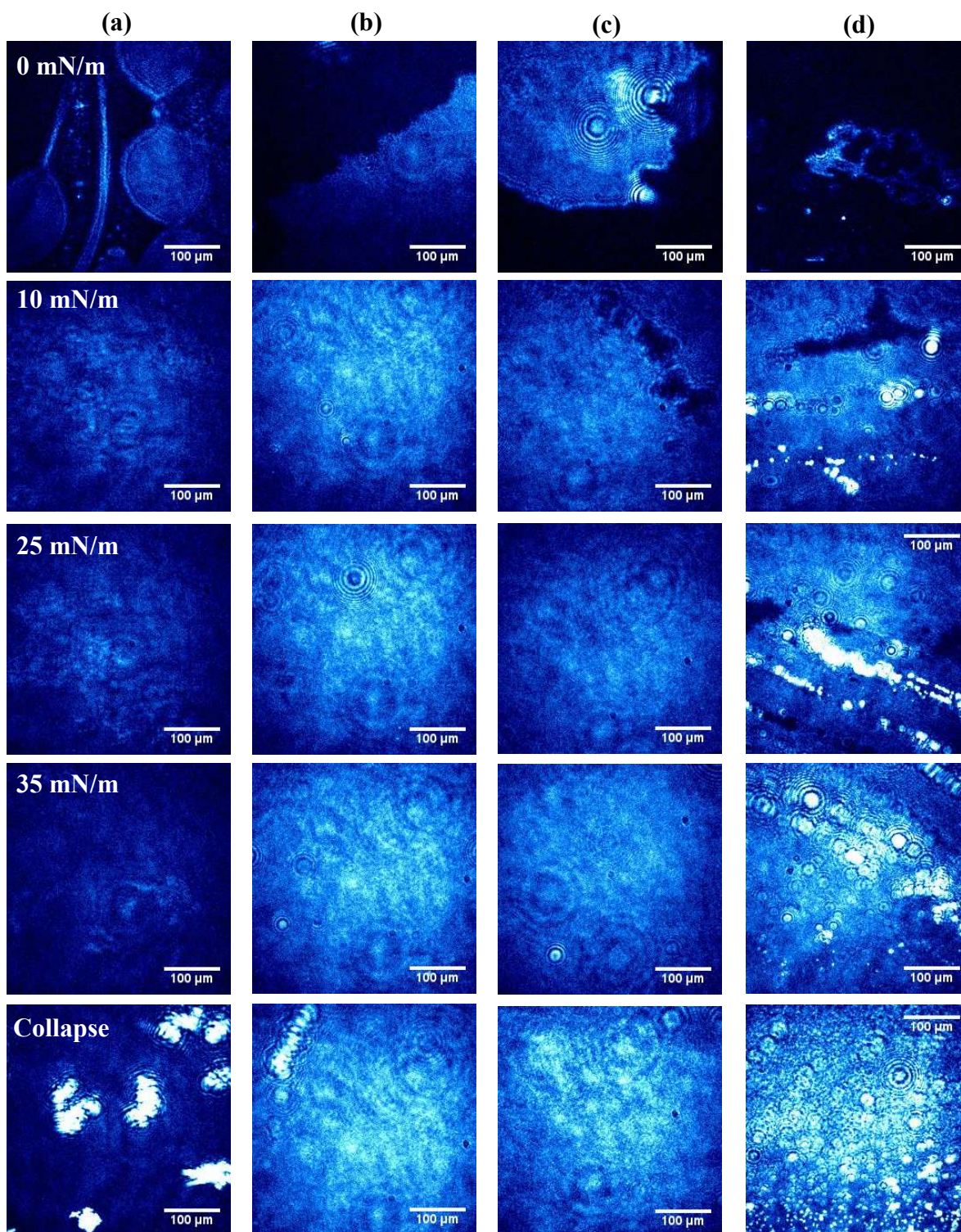
Figure 10: BAM images of PA on (a) pure water; (b) Atlantic seawater, (c) Pacific seawater, and (d) IO. The scale bar of 100 μm and Π at which the image was taken are inset. The Π is constant moving left to right in the figure to compare the various subphases.

4.1.3 Compressibility Modulus

The plots of C^{-1} versus Π for PA on each subphase are shown in Figure 11. In more rigid systems that have a sharp drop in Π at collapse in their isotherms (like PA on pure water) rather than a gradual turn-over, the C^{-1} plot tends towards infinity at high Π values. PA on IO has the lowest C^{-1} values for the majority of Π values, meaning it is the most easily compressed. In the isotherm, this was shown since PA on IO had the most gradual slope in Π with decreasing MMA. However, at $\Pi = 49$ mN/m, C^{-1} increases again, showing the increasing resistance to compression before collapse. The C^{-1} values for PA on Pacific and Atlantic seawater show a similar trend, with Atlantic having less resistance to compression until 43 mN/m when its C^{-1} values surpass those of PA on Pacific. Both these seawater subphases tend towards $C^{-1} = 0$ at high Π. The higher organic content and the large variety of ionic content in Atlantic and Pacific samples could be the reason for their lower C^{-1} values. As the MMA is decreased, the organic matter intertwined in the PA monolayer can be squeezed out rather than the PA molecules having to re-orient. The ions can shield the charges of the partially deprotonated PA headgroups from one another and facilitate closer packing as the MMA is decreased. This is consistent with the lack of phases and compression observed in each isotherm.

The expansion of the IO monolayer from the isotherm rules out closer packing of the PA molecules at the surface as the cause of low C^{-1}, but these ions and organic matter still have a role. The PA is not as strictly bound to the surface on IO, but the molecules that are bound are likely to aggregate, causing low C^{-1}. At IO pH 8.2, some of the PA is able to desorb during compression since its charged headgroup increases water solubility.[14] This enhanced ability to desorb would provide a way for the PA molecules to escape the crowding at the surface without too much of an energy penalty, decreasing the C^{-1}. Regardless of the enhanced ability of PA to

desorb in this system, there still was organic matter on the surface since Π rose as MMA was decreased during the isotherm, and the BAM images evidence major aggregation.
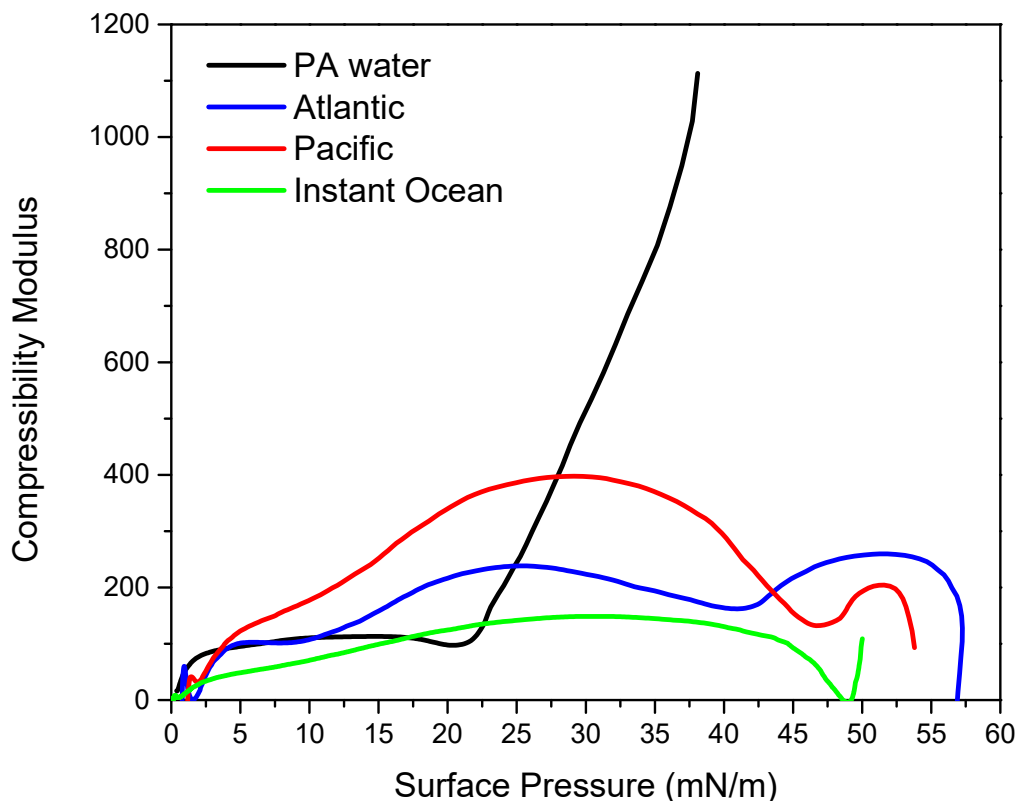
Figure 11: Compressibility modulus values for PA on each subphase.

4.1.4   IRRAS

The IRRAS spectra in the CH and C=O regions of PA on pure water, Atlantic, and Pacific seawater are shown in Figure 12. The only change to note between pure water and Pacific and Atlantic seawaters is the increases in intensities of the ν (CH_2) peaks at 2919 and 2850 cm^{-1} on the real seawater subphases. This shows the enhancement of PA at the surface of real seawater relative to pure water due to the action of pH, organics, and ions in the seawater. The carboxylate region of PA on real seawater is more revealing of the types of surface interactions with this acid. First, the broad positive peak is due to a water bending mode and is present in all

aqueous IRRAS spectra. The hydrated carbonyl peak ν (C=O) at 1722 cm^{-1} on the pure water disappears in the seawater trials, indicating deprotonation. Additionally, the carboxylate carbonyl stretching peak ν (COO$^-$) at 1565 cm^{-1} appears in the real seawater spectra to further evidence the deprotonation of PA that still resides near the interface because of acid-soap complex formation.[29] There is no change in the frequency of δ_s (CH$_2$) = 1469 cm^{-1} between the subphases, indicating PA is in hexagonal packing on all the subphases.[36]
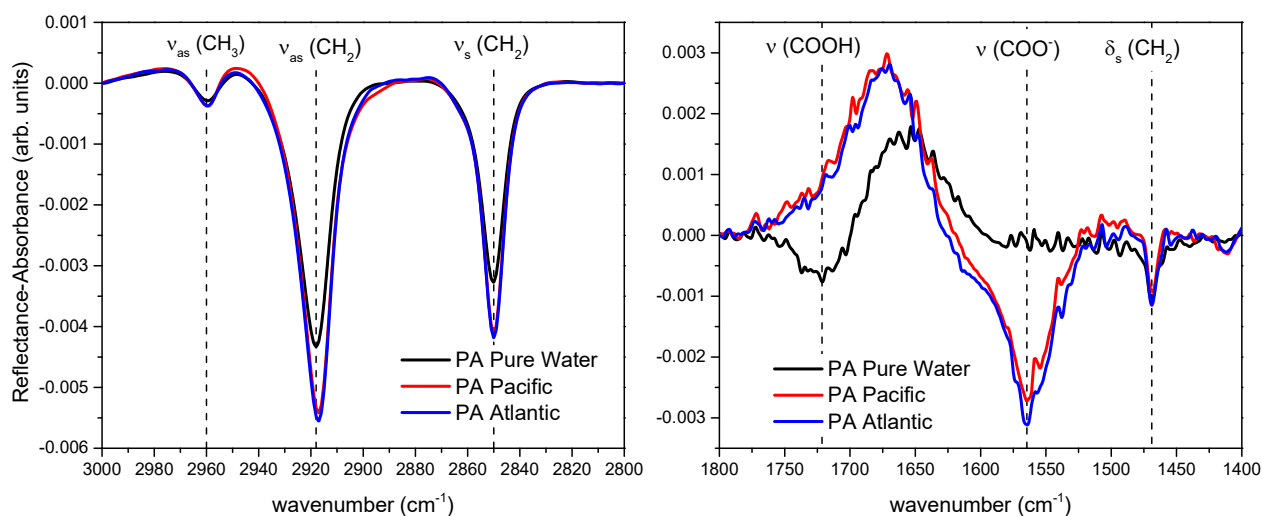

Figure 12: IRRAS in the (left) ν (CH) and (right) ν (C=O) regions of PA on pure water, Atlantic, and Pacific seawater with interesting modes labelled.

The modes on IO are less constant, as shown by the inconsistency between the four trials shown in Figure 13. T1 shows strong CH modes, while the other trials show decreased or no CH modes. This is another example of the inconsistency of IO as a subphase. The aggregation seen in Figure 10 at 10 mN/m on IO could explain this variability: since there are contrasting regions of strong and sparse organic coverage, the IR beam could probe either of these regions between trials, leading to the variable intensities observed. The 1800-1400 cm^{-1} region on IO has many more modes to consider in some trials. A positive mode for the water bend is only seen in T1 and T3, and even so, it does not resemble the bends seen on the other subphases. The water bend

should be present in all aqueous systems, and may not be present in this case due to the subphase. Because of strong aggregation, there could be part of the surface uncovered by surfactant after spreading, meaning the water bending mode would be cancelled through the RA division between background and sample. The most intense peaks from T1 were assigned; while there are many other peaks, there is no need to assign each because of the signal variability and growing disinterest in using IO in future studies. In support of the aggregation idea causing the variable signal, a C=O aggregate stretch was observed at 1698 cm^{-1}.[39] There are two modes observed for the deprotonated carboxylate: the normal at 1575 cm^{-1} and another at 1539 cm^{-1} which corresponds to a COO$^-$ that is interacting with a divalent trace metal.[40,41] The δ_s (CH$_2$) shows a splitting to 1472 and 1463 cm^{-1}, indicating orthorhombic packing[36] in T1 which would be an artifact of the interaction between PA and the many IO components. Some of the inconsistency with IO and real seawater subphases is analyzed deeper in section 4.3.2.
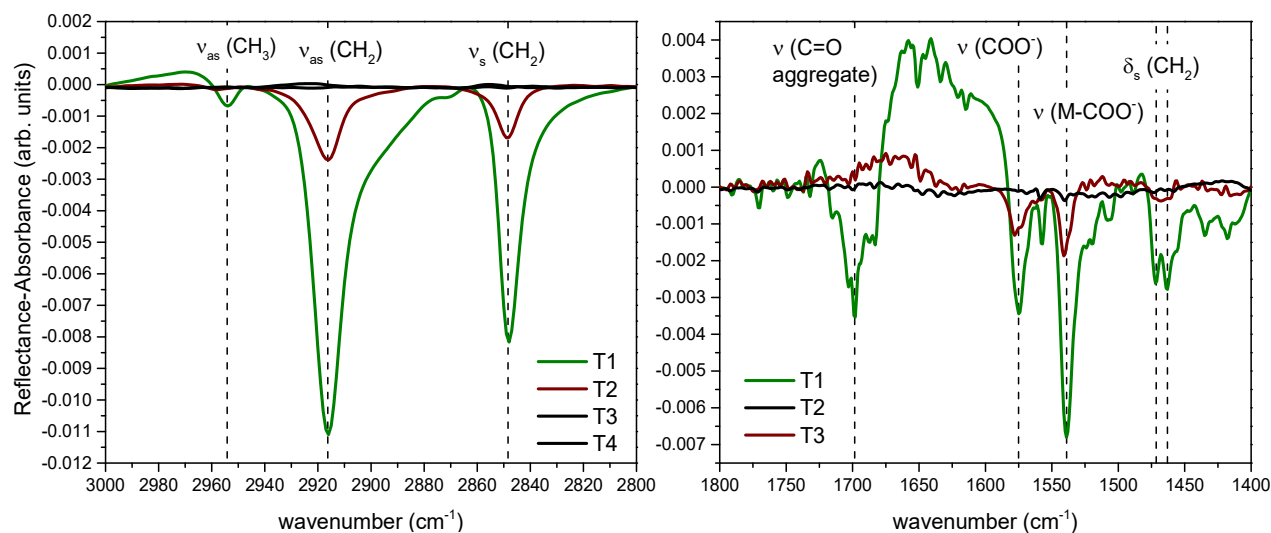

Figure 13: IRRAS in the (left) ν (CH) and (right) ν (C=O) regions of PA on IO with proposed assignments.

4.2 Hexadecanol

4.2.1 Π-A Isotherm

The isotherms of Hex on pure water, Atlantic and Pacific seawaters, and IO are shown in Figure 14. Hex lifts off at 21 Å^2/molecule on pure water,[42] goes through a phase-change from TC to UC at 10 mN/m, then turns over to collapse at 53 mN/m. The monolayer at collapse is less rigid than PA, shown by the gradual turn over to collapse rather than the sharp drop for PA on pure water in Figure 9. Some of the same variability seen in the PA isotherms is also seen in the isotherms in Figure 14, however, this is mainly after collapse. The sharp drops in Π after collapse are due to trough spill over, and this behavior is reproducible with Hex isotherms. The Hex molecule interacts with the subphases differently than PA.

The Hex is less affected by changes in subphase composition than PA. The liftoff of Hex is 23 Å^2/molecule on Atlantic, and 22.5 Å^2/molecule on Pacific, shifting less than 2 Å^2/molecule from pure water. On both the Atlantic and Pacific subphases, the isotherm begins to turn over around 50 mN/m, but then Π rapidly increases before collapsing abruptly. This sort of behavior is indicative of an organic species being "squeezed" out of the monolayer, as seen with PA on Atlantic and Pacific seawater. The structure of the monolayer including this organic species at ~50 mN/m is metastable, but as area decreases further, there is energy benefit for the removal of that species from the monolayer. The Π then rapidly increases as the remaining monolayer condenses, then the stability limit is reached and the monolayer collapses.

Two of the general effects to note are the expansion of the monolayer at liftoff and the lower magnitude of MMA shift at liftoff relative to PA. The expansion of the seawater isotherm relative to water is opposite to the trend seen in the PA isotherms and is explained by the

difference in their molecular head groups. Hex has an alcohol hydrophilic group (Figure 1) with pKa ~ 15, while PA has a carboxylic head group with pKa ~ 5 in bulk solution and 8-9 at the surface.[28,29,43] In the oceanic samples, a pH near 7.6 enables partial deprotonation of PA at the surface, but appreciably no deprotonation of Hex. Because the head group on Hex remains neutral, there are fewer favorable interactions available with the ions in solution, and the molecules cannot pack more closely than on pure water. This lack of interaction is also the cause of the monolayer expansion at liftoff. Surface-active organics in the seawater disrupt the Hex monolayer and cause increases in MMA. There is minimal competition with monolayer-condensing interactions, so the expansion at liftoff is observed. Also of note is the preservation of the phase-change at 10 mN/m from pure water to seawater. This is further evidence of minimal interaction with subphase: the same phases exist on either pure or seawater, so there cannot be any strong interactions that would disrupt monolayer phase.

On IO, the Hex isotherm is very expanded, lifting off near 37.5 $Å^2$/molecule, but there is not as much of an increase in collapse pressure compared to the other subphases as there was with PA on IO. Similar to PA on IO, there is a turn over in the Hex isotherm before another abrupt Π increase. The Hex isotherm turns over near 45 mN/m, then increases sharply near 50 mN/m to turn over again near 60 mN/m. On IO, the phase change is lost, meaning the Hex interacts more strongly with the species in IO than those in the other subphases, which is likely a combination of organic and metal effects. The "true" liftoff point for Hex could not be found when spreading less onto the surface, similar to PA.
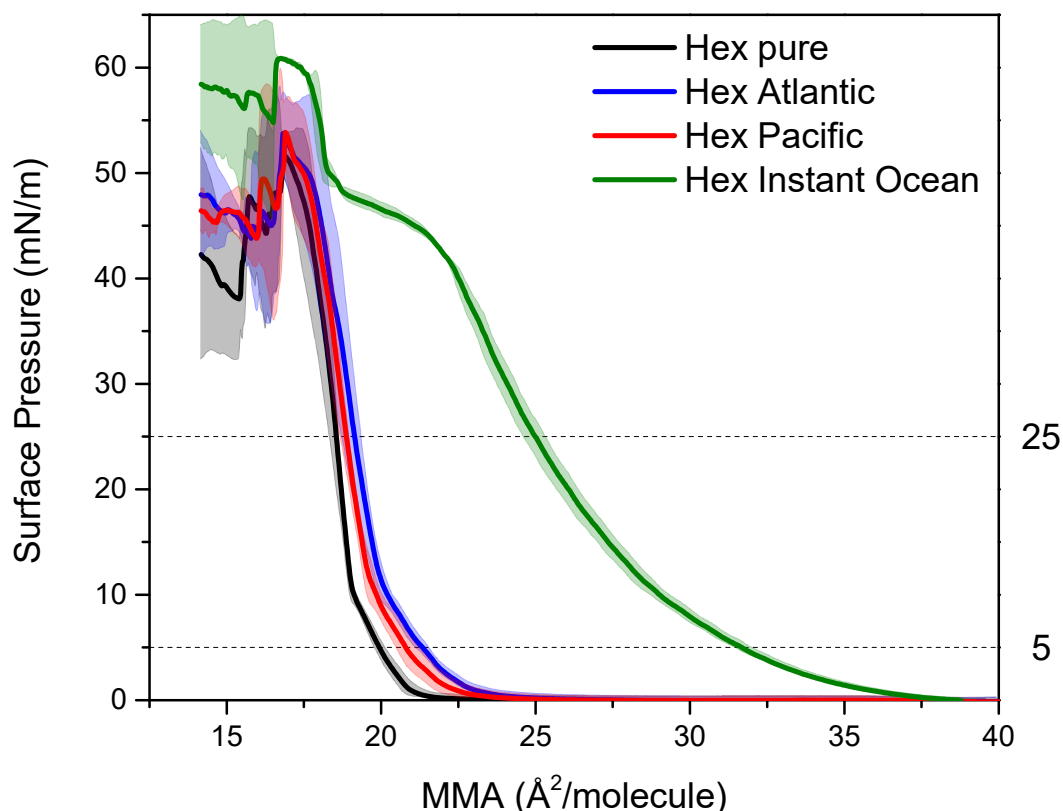
Figure 14: Π-A isotherms of Hex on pure water; Atlantic, and Pacific seawater with horizontal lines showing Π values at which BAM images were taken.

4.2.2 BAM

BAM images of Hex on pure water, Atlantic, and Pacific seawater, and IO are shown in Figure 15. For the majority of images, there is not much difference between the pure water and seawater subphases. Each starts with holes in the surface coverage, then progresses to complete coverage by 5 mN/m, then stays completely covered throughout the acquisition. This is evidence backing the argument about similar interactions between Hex and the three subphases. Since the domains are not visually different for the majority of the isotherm, the interactions producing those domains are likely similar. The most interesting information from the BAM images in Figure 15 is the formation of 3D domains in the collapse of the Pacific trial. The more abrupt collapse seen in the seawater samples in Figure 14 could indicate the formation of 3D aggregates

to quickly lower the energy of the system, and this is confirmed via BAM. A 3D aggregate is not imaged in the Atlantic trial, but there is a visible fold in the monolayer, shown as a streak of bright bordered by darker regions. This indicates some conformational change at collapse that must decrease the energy of the system.

On IO, there are small bright specs visible in each frame, indicating some type of aggregation, different from the PA aggregates on IO. This reinforces that the lipid plays a role in aggregate formation rather than it being only a subphase effect. At 25 mN/m, the monolayer shows different behavior from the other subphases at the same Π because there are regions of lipid depletion on IO rather than a sheet as on the other subphases. The BAM images from Π values corresponding to either turn over at 45 or 60 mN/m are the same. At collapse, there are no large aggregates, unlike on the Pacific water. This could mean the monolayer can reorganize better than on the other subphases since 3D domains do not have to be formed to maintain the monolayer at the surface. The isotherm was expanded, but Hex could dissociate into the bulk, accommodated by IO species, rather than folding onto itself as it had to on Pacific and Atlantic seawater.
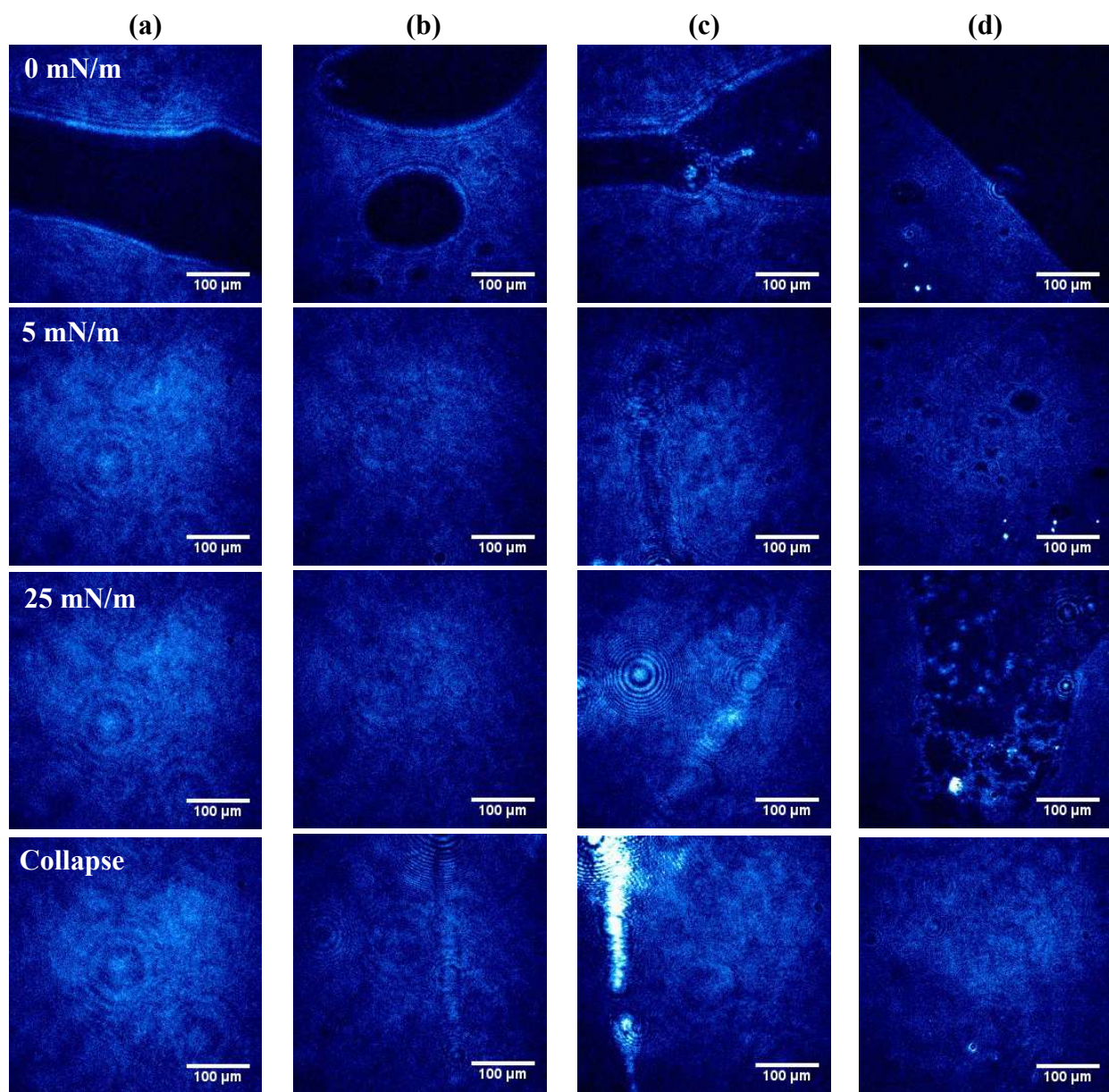
Figure 15: BAM images of Hex on (a) pure water; (b) Atlantic seawater, (c) Pacific seawater, and (d) IO. The scale bar of 100 μm and Π at which the image was taken are inset. The Π is constant moving left to right in the figure to compare the various subphases.

4.2.3 Compressibility Modulus

In Figure 16 the C^{-1} for Hex on pure water, Atlantic and Pacific seawaters, and IO is plotted versus Π. While the C^{-1} plot for PA was rather incompressible at high Π, hexadecanol has a gradual turn over into collapse, so its C^{-1} tends towards zero at high Π. The same trend of C^{-1} for PA is shown with Hex, that on IO Hex has the least resistance to compression, and an increasing resistance from Atlantic to Pacific to pure water. While for PA real seawater the C^{-1} values tended towards zero at high Π, near 51 mN/m the C^{-1} for Hex on these subphases starts to increase again. Since Hex has a headgroup that has more limited interaction with the bulk, it becomes less compressible at these high Π values. In the IO trace, the C^{-1} starts increasing at 47 mN/m, so the different organic and ion content in IO causes the Hex to be less compressible at a lower Π than real seawater.
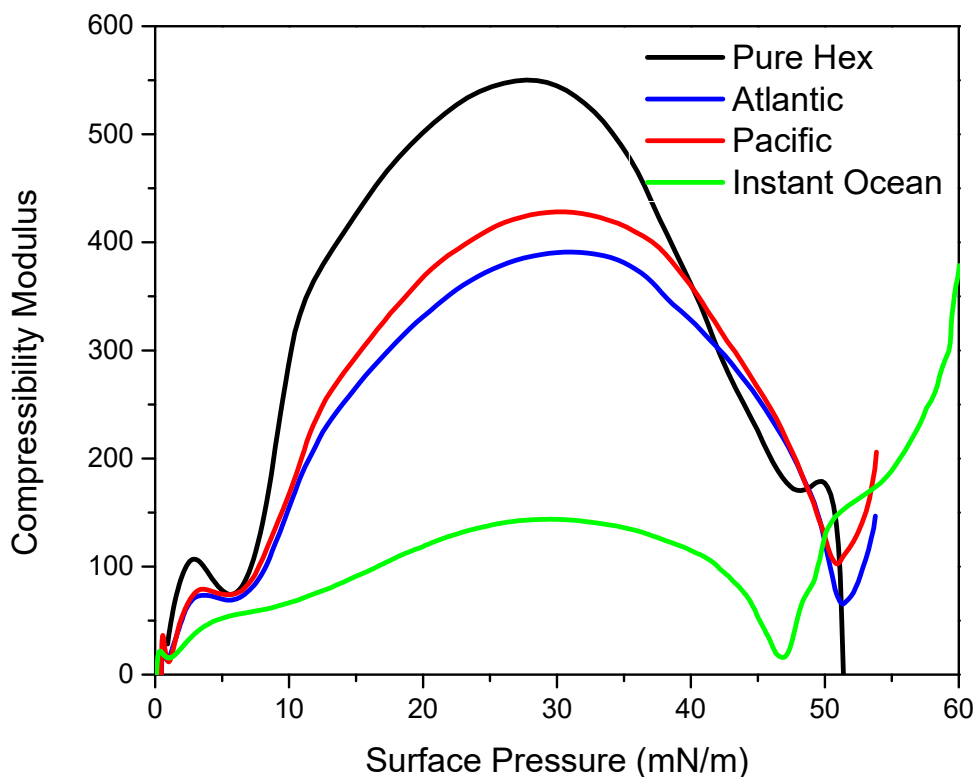

Figure 16: C^{-1} versus Π of Hex on pure water, Atlantic and Pacific seawaters, and IO.

4.2.4 IRRAS

Unlike the PA CH region, there are no significant changes to note between Hex on pure water versus the real seawaters in the CH region, as seen in Figure 17. Each of the CH modes shown has the same wavenumber and similar intensity regardless of subphase. The 1800-1400 cm^{-1} regions on pure water, and Atlantic and Pacific seawaters show only the positive water bend and δ_s (CH$_2$) = 1469 cm^{-1} that does not change between subphases on Atlantic or Pacific seawater. While hexadecanol has been reported to pack orthorhombically at the interface to induce ice nucleation in aerosol particles,[18,44] splitting of the δ_s (CH$_2$) mode to indicate orthorhombic packing[36] was not observed here.
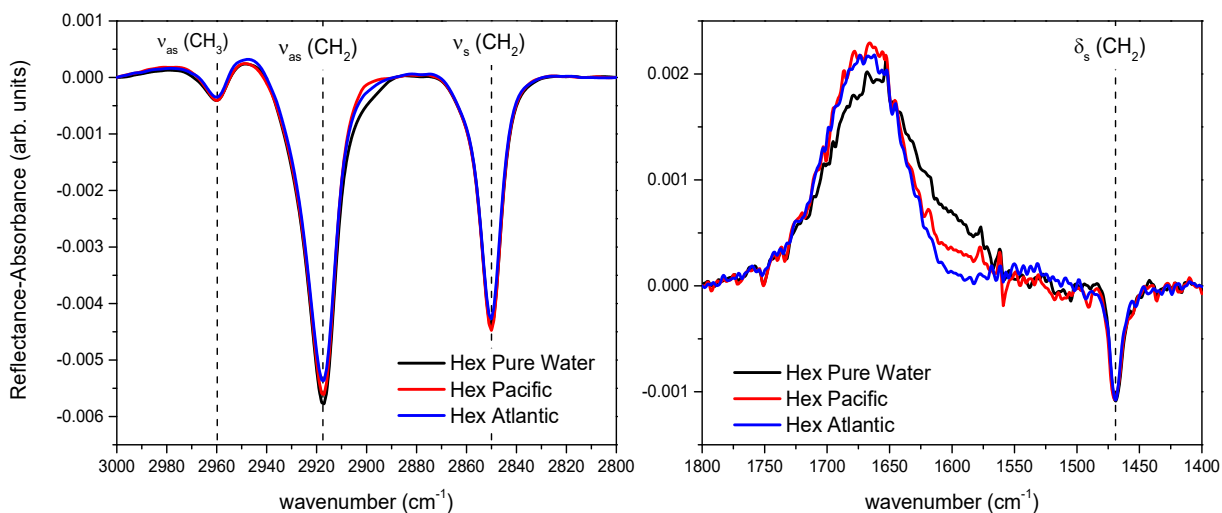

Figure 17: IRRAS in the (left) ν (CH) and (right) δ (CH) regions of Hex on pure water, Atlantic, and Pacific seawaters.

On IO, the Hex CH peaks did have variable intensity, but not as much as they did with PA. These peaks show no major frequency shifts compared to pure water. The δ_s(CH$_2$) region is more noisy and inconsistent. There is no water bend observed similar to the PA trials, and the broad band at 1530 cm^{-1} in T2 and T3 cannot be confidently assigned, but could be an artifact from RA calculation on IO. Since IO has independently surface-active organics, if the IR beam

impinged organics in the R_o spectrum and not in the R spectrum (from aggregation), this behavior could result. In T1, there are two modes at 1473 and 1457 cm^{-1} labelled as δ_s (CH$_2$) that would indicate orthorhombic packing due to species within IO, but this could just be noise. The broad 1530 cm^{-1} band obscures the δ_s (CH$_2$) in the other trials.
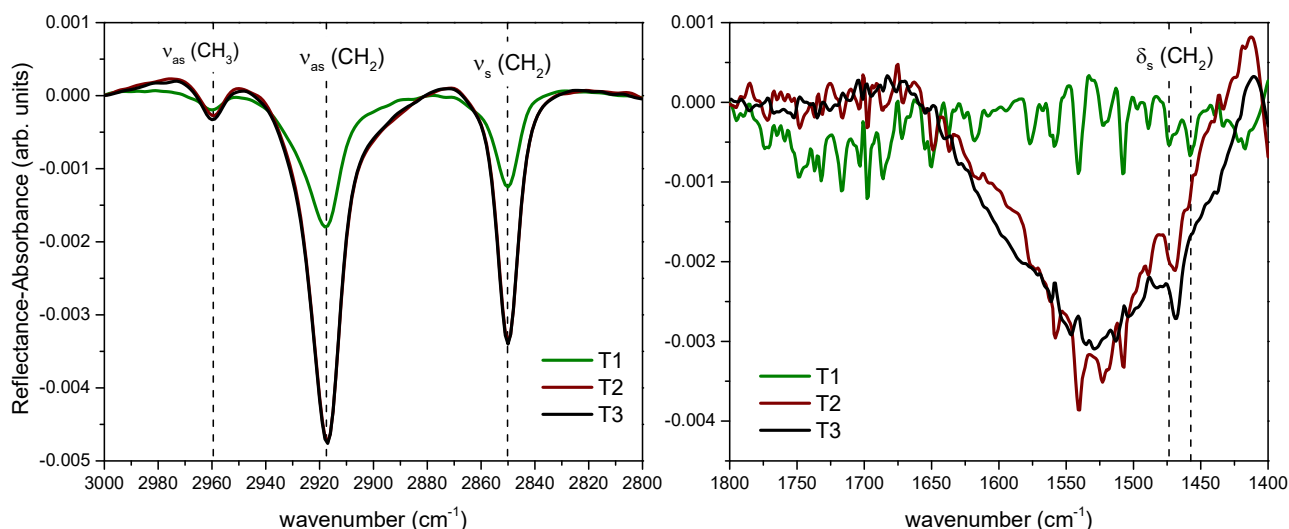

Figure 18: IRRAS of Hex on IO in the (left) CH region and (right) δ_s (CH$_2$) region .

4.3 Cautions to consider when using real seawater samples

4.3.1   Real Seawater

The variability in the Atlantic and Pacific seawater isotherms for PA (Figure 9) is due to the nature of real seawater samples: seawater contains a large array of organic and inorganic species, and it is difficult to ensure each aliquot of sample used in a trial will contain the same amount of each species, even when agitating the sample prior to use. If more organics enter the subphase aliquot on a specific trial, the isotherm may show more expansion than another, for example. Additionally, humidity effects, which are more easily noticed in the organic-rich oceanic samples, can alter the isotherm shape.[45] Isotherms on Atlantic and Pacific ocean water had completely different shapes at relative humidity 35% versus 28%, as shown in Figure 19,

45

which compares PA on pure water to PA on Pacific seawater under two different external conditions. The two Pacific traces share a similar liftoff point indicating similar monolayer behavior prior to liftoff. However, as Π increases, the higher humidity trace shows expansion relative to the lower humidity trial. Additionally, the higher humidity trace collapses at a lower Π. A similar effect was seen with the Atlantic seawater isotherms. This is the main reason for the higher standard deviation in the Atlantic and Pacific seawater isotherms, especially in the collapse region.
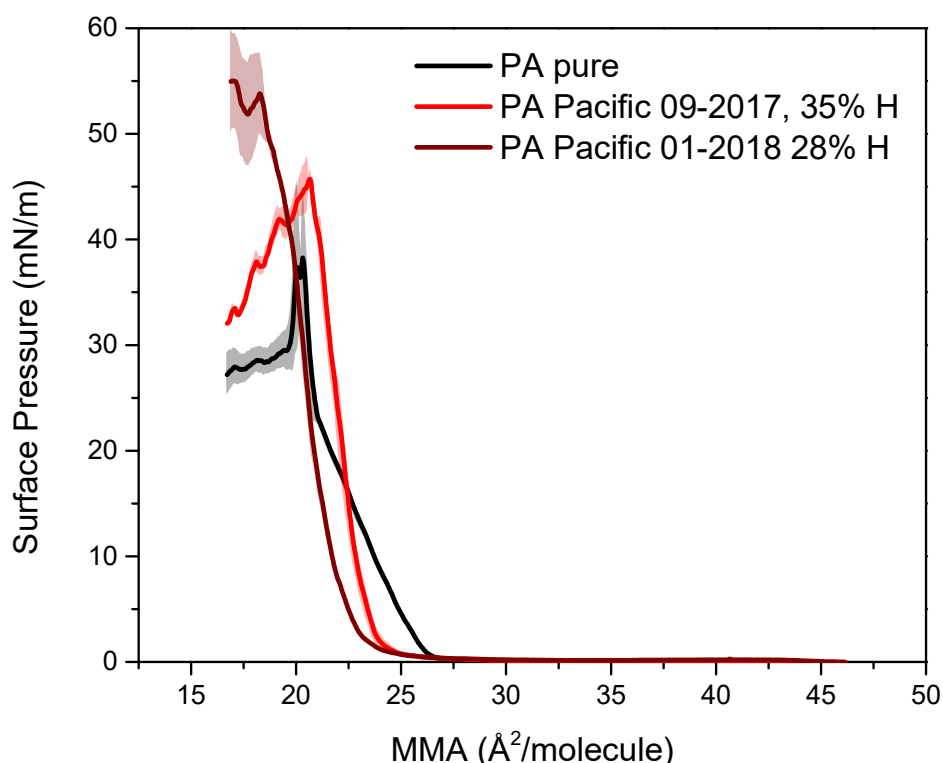
Figure 19: Π-A isotherms of PA on Pacific seawater showing the difference in isotherm shape dependent on subphase composition and humidity.

In addition to humidity and aliquot considerations, the seawater samples showed changes in pH over time that could alter isotherm shape. While oceanic pH is ~8.1, the Atlantic sample was pH 7.66 ± 0.07 and the Pacific was pH 7.53 ± 0.07 when measured in 2018, over a year and a half after collection. This apparent drop in pH could be attributed to the respiratory activity of

microbes in the samples. Microbial respiration cycles can produce compounds such as ammonium or phosphate that alter the pH of water.[46] Ammonium is acidic and decreases the pH, while phosphate lowers the buffering capacity, making the system more susceptible to pH changes. In the ocean, these effects are balanced through the circulation of water to replenish depleted or remove excess species,[46] but in the closed samples used here, these effects have no balancing force. Microbial nutrient cycling occurs quickly, so these changes are feasible by the time the pH of these samples was taken. While the seawater samples were refrigerated, this treatment only slows microbial activity. In the future, the kinetics of seawater acidification should be tracked from the moment the samples are obtained through their use and storage.

4.3.2   Instant Ocean Seawater

Following the extensive techniques applied to analyze samples on an IO subphase, it is suggested that a house-made seawater is more appropriate for analysis in the Allen lab. Many, if not all the experiments conducted are extremely sensitive to organic contamination, and the amount present in IO prohibits its utility. First, isotherms of either lipid on IO were far expanded. This major expansion is due to surface crowding by the organic content of IO, which is only 29 ppm,[31] but has an effect on the monolayers here. The species used to manufacture organic content in IO could be different than those naturally occurring in seawater, causing the difference. The surface tension of pure water was 71.05 mN/m, Atlantic was 73.98 mN/m, Pacific was 75.03 mN/m, and IO was 56.47 mN/m, all at 22.6 ± 0.1 °C and 40 ± 1 % RH. The increase in ST of the oceanic samples relative to pure water is due to the ordering of water with salt presence.[20] The great decrease in γ in the IO sample is complementary evidence of extensive surfactant contamination. When sweeping the surface to ensure cleanliness prior to an isotherm experiment, on IO the Π would rise irreproducibly no matter how many times the surface was

aspirated. Additionally, the BAM images of IO without a lipid on the surface showed organic content. There may be value in trying to remove organics from the IO crystals prior to dissolution, but this idea was not evaluated herein. Another study rinsed IO crystals with dichloromethane then dried them prior to dissolution, and found a condensation of PA on IO relative to pure water.[47] However, in this study, Π was determined via an iterative compression method in which readings were taken discretely at certain barrier positions prior to further compression. This practice could give rise to metastable states from which dissolution could occur between readings, causing the discrepancy between the data obtained here.

Even when spreading less lipid on the surface for an isotherm, a "true" liftoff point (where Π is zero reproducibly for >10 $Å^2$/molecule prior to liftoff) could not be determined, as shown in Figure 20 with PA. The monolayer shows different mechanisms of liftoff depending on the starting area between the molecules, showing a turn over near 40 mN/m with 20 μL spread, and a much more gradual lift off slope with 5 μL spread. While the IO solutions used as subphases for the figures presented here were prepared in tap water, there was no major change in isotherm characteristics when using ultrapure water for IO preparation. Since the ionic and organic content of IO is so high, the ions and organics introduced from tap water do not affect the dynamics of the lipid.
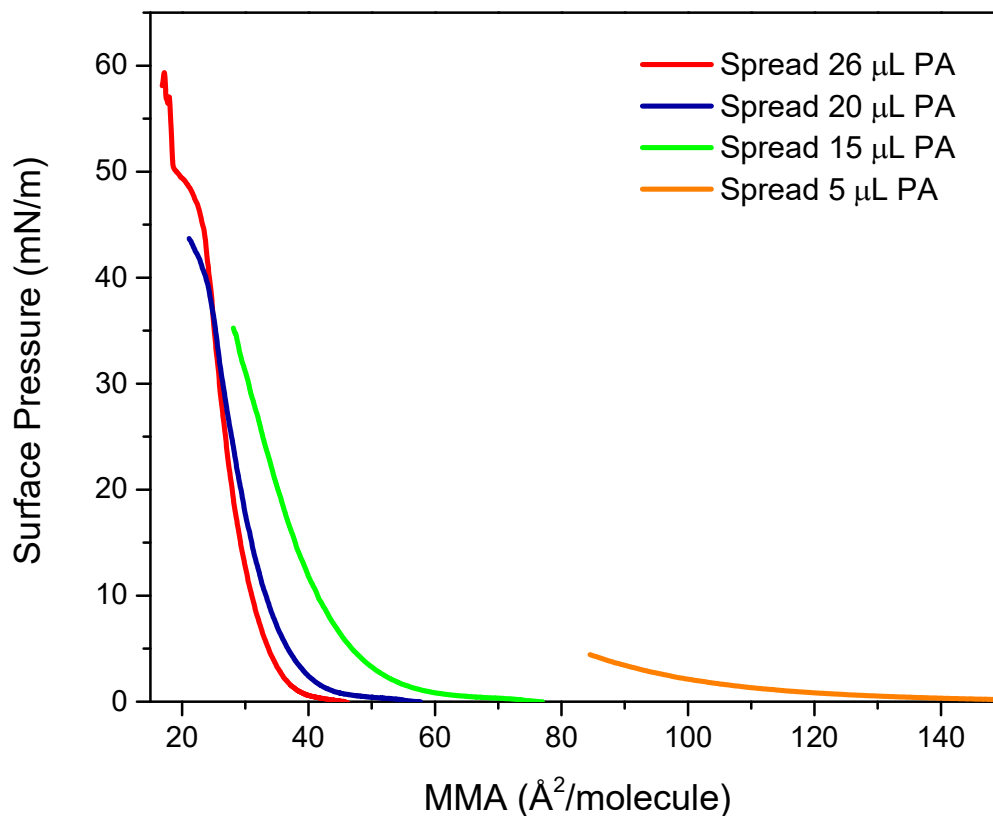
Figure 20: Π-A isotherms of PA on IO: less PA was spread onto the IO subphase and the Π lifted off almost immediately after compression started.

As noted, the pH of the real ocean samples was lower than 8.2, so the IO was pH adjusted with HCl to pH 7.7 to determine if the isotherm expansion was a pH effect. As shown in Figure 21, the pH was not the cause. The minor differences in isotherm shape between the IO trials could be due to the ΔpH of 0.5 but are more likely due to the inherent error of the experiment.
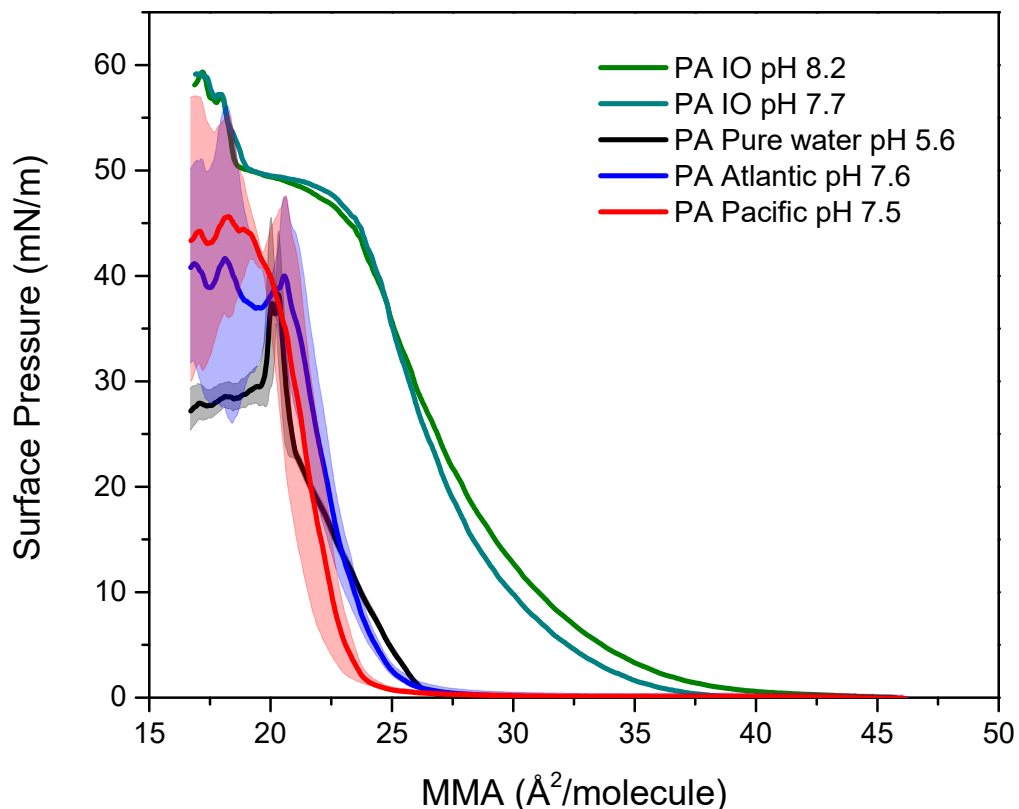
Figure 21: The pH adjusted IO isotherm matches the original, meaning the expansion of the IO monolayer was not due to the pH difference between pure water or real seawater.

A better proxy based on initial results would be "homemade" artificial seawater, containing $NaCl$, $CaCl_2$, $MgCl_2$, and $NaOH$ to adjust the pH. The preliminary results from this system are presented in Appendix 1: Initial Results on House-Made ASW. Unfortunately, the pH is hard to maintain in this system, and the results presented in the appendix do not have pH data supporting a pH of 8.2.

Chapter 5: Conclusions

To study the fundamental physicochemical interactions of atmospherically relevant lipids in the lab, a suitable proxy system must be determined to strip down the complexity of real-world seawater samples. Organics, ions, and pH are just some of the factors that affect the surface interactions of surfactants, so controlling certain variables allows for stronger conclusions in the lab. PA is found in the SSML and is enhanced in SSA, while Hex is produced from the microbial breakdown of larger organics and is an efficient ice nucleator. These lipids are effective stand-in species to evaluate different proxy subphases.

From Π-A isotherms, BAM images, and IRRAS spectra, the following conclusions have been determined. PA interacts more strongly with each subphase evaluated than Hex. On real seawater, a PA monolayer is condensed at low Π relative to pure water, while expanded on IO. On seawater, the combination of pH with ionic effects cause this condensation until the organics in the samples cause expansion at higher Π before they are squeezed out of the monolayer. On the real seawaters and IO, the phase change in PA is lost, exhibiting the strong interactions between PA and subphase species. On IO, PA tends to aggregate even at low Π and is most compressible. PA shows hexagonal packing on all subphases. Hex monolayers are expanded on each seawater subphase relative to water, but are much more expanded on IO than real seawater. The phase change in the monolayer is maintained in real seawater, while lost in IO, showing stronger Hex interaction with IO species. Hex may show orthorhombic packing on IO, but the noise within IRRAS spectra prevent confident conclusions. On all subphases for both lipids, the monolayers collapse at a higher Π than on pure water, showing the ability for tighter molecular packing at high Π in each case.

Because of the uncertainty in experiments with IO and its failure to reproduce the behavior on real seawater, its use as a subphase is unsuitable in the Allen lab. The organic content of IO is unknown and the trace metal species may be introduced to the product in forms that do not occur in nature, causing the differential behavior between IO and real seawater. House-made ASW preliminarily gave the most matching results to real seawater samples, but the sample preparation and maintenance have not been optimized to allow for its efficient use at the time of this thesis. Although a "perfect" model system was not found, one possiblity has been eliminated, so future work may more efficiently work towards applying fundamental lab study to real climate-influencing environments.

References

1. Rosen, M. J.; Kunjappu, J. T. Characteristic Features of Surfactants. In *Surfactants and Interfacial Phenomena,* Wiley: Hoboken, N.J., 2012; pp 1.

2. Donaldson, D. J.; Vaida, V. The influence of organic films at the air-aqueous boundary on atmospheric processes. *Chem. Rev.* **2006***, 106*.

3. Cunliffe, M. et al. Sea surface microlayers: A unified physicochemical and biological perspective of the air-ocean interface. *Progress in Oceanography.* **2013***, 109*, 104-116.

4. Resch, F.; Afeti, G. Film drop distributions from bubbles bursting in seawater. *Journal of Geophysical Research: Oceans.* **1991***, 96*, 10681-10688.

5. Cochran, R. E.; Jayarathne, T.; Stone, E. A.; Grassian, V. H. Selectivity Across the Interface: A Test of Surface Activity in the Composition of Organic-Enriched Aerosols from Bubble Bursting. *J. Phys. Chem. Lett.* **2016***, 7*, 1692-6.

6. Charlson, R. J. Climate Forcing by Anthropogenic Aerosols. *Science* **01***, 255*, 423-430.

7. Liepert, B. G. The physical concept of climate forcing. *Wiley Interdisciplinary Reviews: Climate Change.* **2010***, 1*, 786-802.

8. Kiehl, J. T.; Briegleb, B. P. The relative roles of sulfate aerosols and greenhouse gases in climate forcing. *Science.* **1993***, 260*.

9. Boucher, O. D. et al. Clouds and Aerosols. In *Climate Change 2013: The Physical Science Basis*; Stocker, T. F., D. Qin, G., Plattner, M., Tignor, S. K., Allen, J., Boschung, A., Nauels, Y., Xia, V. B. and Midgley, P. M., Eds.; Cambridge University Pres: Cambridge, UK and New York, NY, USA, 2013; pp 571.

10. Liepert, B. G. Observed reductions of surface solar radiation at sites in the United States and worldwide from 1961 to 1990. *Geophysical Research Letters.* **2002***, 29*, 61-1-61-4.

11. Petty, M. C. *Langmuir-Blodgett films: An Introduction;* Cambridge University Press: Cambridge; New York, 1996; , pp 234.

12. Cochran, R. E. et al. Analysis of Organic Anionic Surfactants in Fine and Coarse Fractions of Freshly Emitted Sea Spray Aerosol. *Environ. Sci. Technol.* **2016***, 50*, 2477-86.

13. Ciuraru, R. et al. Photosensitized production of functionalized and unsaturated organic compounds at the air-sea interface. *Sci. Rep.* **2015***, 5*.

14. Adams, E. M. et al. Sodium-carboxylate contact ion pair formation induces stabilization of palmitic acid monolayers at high pH. *Phys. Chem. Chem. Phys.* **2017***, 19*, 10481-10490.

15. Sattler, B.; Puxbaum, H.; Psenner, R. Bacterial growth in supercooled cloud droplets. *Geophysical Research Letters.* **2001***, 28*, 239-242.

16. Cochran, R. E. et al. Molecular Diversity of Individual Sea Spray Aerosol Particles: Influence of Ocean Biology on Particle Composition and Hygroscopicity. *Chem.* **2017***, 2*, 655.

17. Cantrell, W.; Robinson, C. Heterogeneous freezing of ammonium sulfate and sodium chloride solutions by long chain alcohols. *Geophysical Research Letters* **2006**, *33*.

18. Qiu, Y. et al. Ice Nucleation Efficiency of Hydroxylated Organic Surfaces Is Controlled by Their Structural Fluctuations and Mismatch to Ice. *J. Am. Chem. Soc.* **2017**, *139*, 3052-3064.

19. Nguyen, C. V.; Phan, C. M.; Nakahara, H.; Shibata, O. Surface structure of sodium chloride solution. *J. Mol. Liq.* **2017**, *248*, 1039-1043.

20. Jungwirth, P.; Tobias, D. J. Molecular structure of salt solutions: a new view of the interface with implications for heterogeneous atmospheric chemistry. *J. Phys. Chem. B.* **2001**, *105*.

21. Götte, L. et al. Solvent-Shared Ion Pairs at the Air-Solution Interface of Magnesium Chloride and Sulfate Solutions Revealed by Sum Frequency Spectroscopy and Molecular Dynamics Simulations. *J. Phys. Chem. A.* **2017**, *121*.

22. Petersen, P. B.; Saykally, R. J. On the Nature of Ions at the Liquid Water Surface. *Annu. Rev. Phys. Chem.* **2006**, *57*.

23. Garrett, B. C. Ions at the Air/Water Interface. *Science.* **2004**, *303*.

24. Knipping, E. M. et al. Experiments and Simulations of Ion-Enhanced Interfacial Chemistry on Aqueous NaCl Aerosols. *Science.* **2000**, *287*.

25. Casillas-Ituarte, N. N. et al. Surface organization of aqueous $MgCl_2$ and application to atmospheric marine aerosol chemistry. *PNAS.* **2010**, *107*, 6616-6621.

26. Tang, C. Y.; Huang, Z.; Allen, H. C. Binding of Mg^{2+} and Ca^{2+} to palmitic acid and deprotonation of the COOH headgroup studied by vibrational sum frequency generation spectroscopy. *J. Phys. Chem. B.* **2010**, *114*, 17068-76.

27. Skop, R. A.; Tseng, R.; Brown, J. W. Effects of salinity and surface tension on microbubble-mediated sea-to-air transfer of surfactants. *Journal of Geophysical Research: Oceans.* **1993**, *98*, 8489-8494.

28. Wellen, B. A.; Lach, E. A.; Allen, H. C. Surface pKa of octanoic, nonanoic, and decanoic fatty acids at the air-water interface: applications to atmospheric aerosol chemistry. *Phys. Chem. Chem. Phys.* **2017**, *19*, 26551-26558.

29. Kanicky, J. R.; Shah, D. O. Effect of Premicellar Aggregation on the pKa of Fatty Acid Soap Solutions. *Langmuir.* **2003**, *19*, 2034-2038.

30. Millero, F. J. *Chemical oceanography;* CRC/Taylor and Francis: Boca Raton, 2006; .

31. Atkinson, M. J.; Bingman, C. Elemental composition of commercial seasalts. *Journal of Aquariculture and Aquatic Sciences* **1998**, *8*, 39.

32. Gentle, I.; Barnes, G. *Interfacial science : an introduction;* Oxford University Press: Oxford, New York, 2005; .

33. Osvaldo, O. Langmuir-Blodgett films-properties and possible applications. *Braz. J. Phys.* **1992**, *22*, 60.

34. Vollhardt, D.; Fainerman, V. B. Progress in characterization of Langmuir monolayers by consideration of compressibility. *Adv. Colloid Interface Sci.* **2006**, *127*, 83-97.

35. Bordo, V. G.; Rubahn, H. -. *Optics and spectroscopy at surfaces and interfaces;* Wiley-VCH: Weinheim, 2005; , pp 272.

36. Mendelsohn, R.; Flach, C. R.; Griffiths, P. R. Infrared Reflection - Absorption Spectrometry of Monolayer Films at the Air - Water Interface. **2006**.

37. Pilson, M. E. Q. *An Introduction to the Chemistry of the Sea;* Prentice Hall: 1998; , pp 431.

38. Adams, E. M.; Allen, H. C. Palmitic Acid on Salt Subphases and in Mixed Monolayers of Cerebrosides: Application to Atmospheric Aerosol Chemistry. *Atmosphere* **2013**, *4*, 315-336.

39. Goto, T. E.; Caseli, L. Understanding the collapse mechanism in Langmuir monolayers through polarization modulation-infrared reflection absorption spectroscopy. *Langmuir.* **2013**, *29*, 9063-71.

40. Gericke, A.; Mendelsohn, R. Partial Chain Deuteration as an IRRAS Probe of Conformational Order of Different Regions in Hexadecanoic Acid Monolayers at the Air/Water Interface. *Langmuir.* **1996**, *12*, 758-762.

41. Gericke, A.; Huehnerfuss, H. The effect of cations on the order of saturated fatty acid monolayers at the air-water interface as determined by infrared reflection-absorption spectrometry. *Thin Solid Films.* **1994**, *245*, 74.

42. Gopal, A.; Ka Y.; Lee, K. Y. C. Headgroup percolation and collapse of condensed Langmuir monolayers. *J. Phys. Chem. B.* **2006**, *110*.

43. McLean, D. S.; Vercoe, D.; Stack, K. R.; Richardson, D. The colloidal pKa of lipophilic extractives commonly found in Pinus radiata. *Appita.* **2005**, *58*, 362-366.

44. Popovitz-Biro, R. et al. Induced freezing of supercooled water into ice by self-assembled crystalline monolayers of amphiphilic alcohols at the air-water interface. *J. Am. Chem. Soc.* **1994**, *116*.

45. Zuo, Y. Y. et al. Effect of humidity on the adsorption kinetics of lung surfactant at air-water interfaces. *Langmuir.* **2005**, *21*, 10593-601.

46. Sigman, D. M.; Hain, M. P. The Biological Productivity of the Ocean. *Nature Education* **2012**, *3*, 21.

47. Lindsley, W. G.; Skop, R. A.; Brown, J. W. Surface pressure and wave-damping effects of surface-active organic compounds on seawater. *Ocean Engineering.* **1991**, *18*, 593-601.

Appendix 1: Initial Results on House-Made ASW

While the majority of data presented is on pure water, Atlantic and Pacific seawaters, and IO, the formula used for lab-made artificial seawater is worth describing because preliminary results on this subphase most closely matched real seawater trials. This artificial seawater (ASW) was created by a recipe from Chemical Oceanography by Frank Millero, with 0.47 M NaCl, 0.05 M $MgCl_2$, and 0.01 M $CaCl_2$ at pH 8.2.[30] The NaCl was massed in as a solid while the $MgCl_2$ and $CaCl_2$ were added from stock solutions that had been filtered through activated carbon thrice then standardized via Mohr titration. A stock solution of NaOH was used to adjust the pH. This ASW solution was the most difficult to create and store. First, the high ionic strength caused a resistance to pH change when initially making the solution that made addition volumes hard to predict. Second, the NaOH stock was initially kept in volumetric glassware and likely leeched residual chemicals from this glassware, causing subsequent ASW solutions to be contaminated and results to be irreproducible.

The isotherms in Figure 22 are those obtained for PA and Hex on the house-made ASW. Due to limitations in the way the ASW was prepared (pH; contamination over time from NaOH leeching glassware), these cannot be confidently called the best way to model oceanic subphases in the lab. The trials presented do match well with the Atlantic and Pacific seawaters though, showing monolayer condensation with PA and expansion with Hex on the same magnitudes as on real seawater.
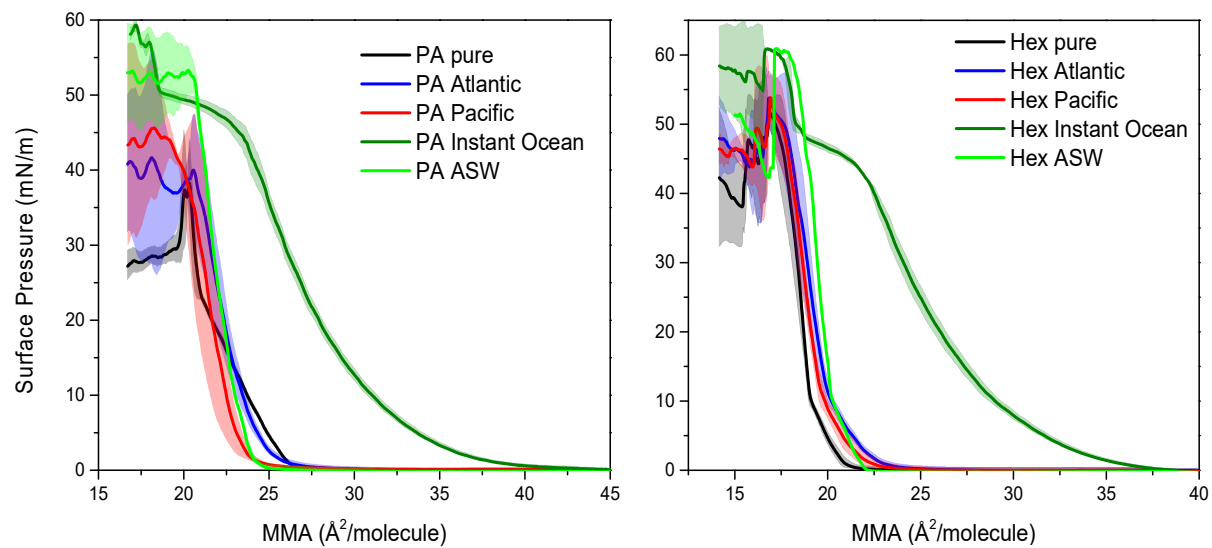
Figure 22: Π-A isotherms of PA and Hex on house-made ASW preliminarily match isotherms on real seawater the best.

Appendix 2: Peak Analysis in Origin

This appendix contains instructions and screenshots covering how to baseline subtract spectra in Origin using a built-in tool. With the plot of interest selected, choose Analysis => Peaks and Baseline => Peak Analyzer => Open Dialogue.
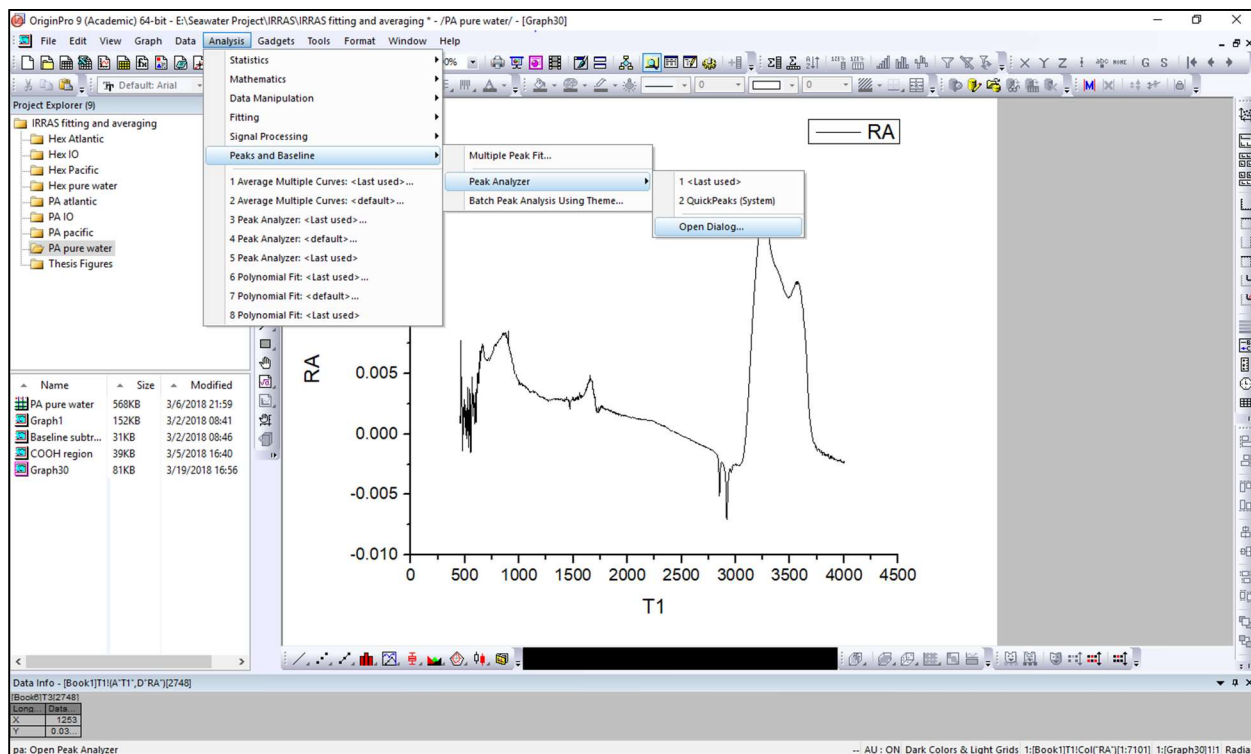

Change Recalculate to Auto, Goal to Subtract Baseline, and expand the Input section, and choose By X and enter the region you want to have subtracted.
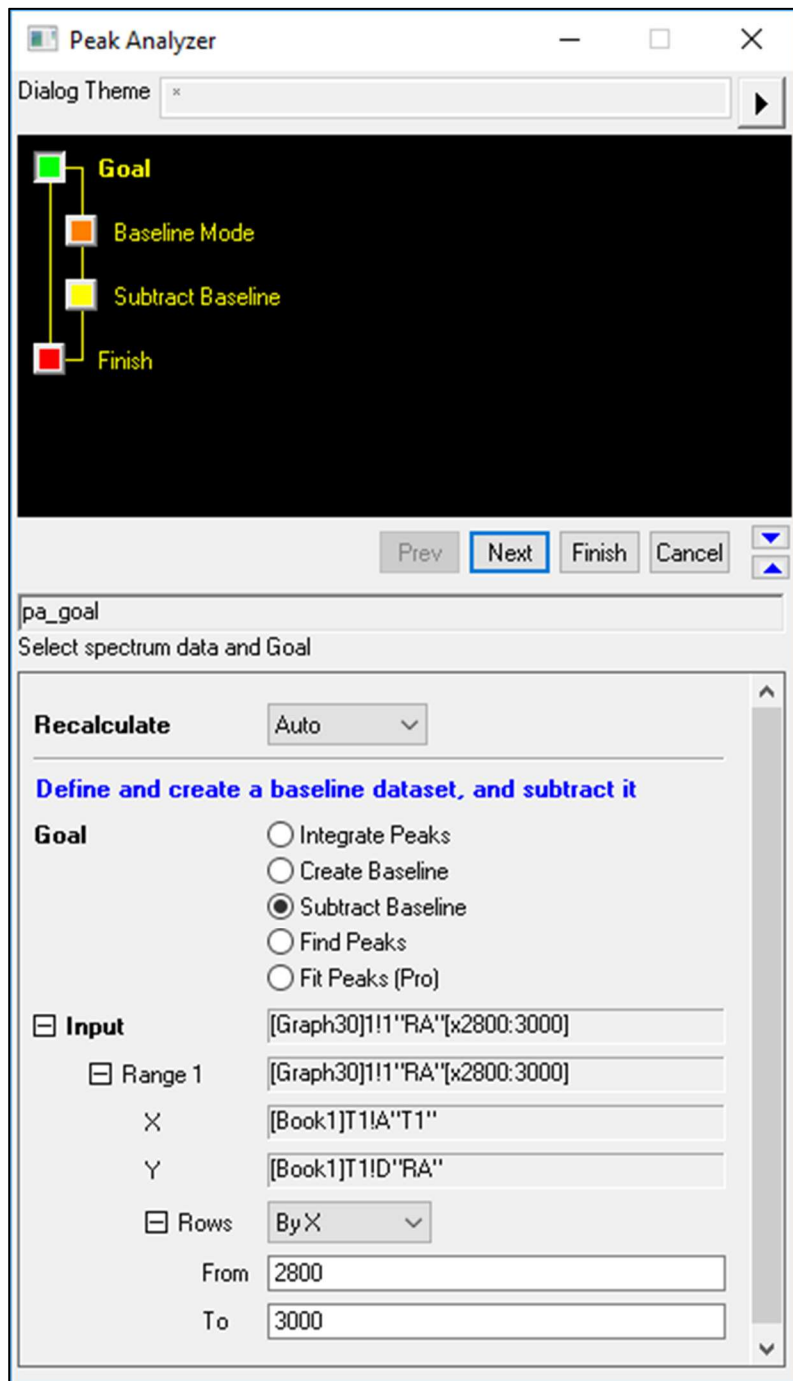
There will be a temporary graph in the background that shows the current spectral region you have chosen that you can use to visualize what changes you make. Choose next. Change Baseline Mode to User Defined then click Find to have Origin find what points the program thinks are your baseline. You can change the number of points you want to use to define your

baseline with the Number of Points to Find box. If certain points are not placed correctly, choose Modify/Del then drag the points to correct locations within that temporary graph mentioned earlier. When satisfied, click Next.
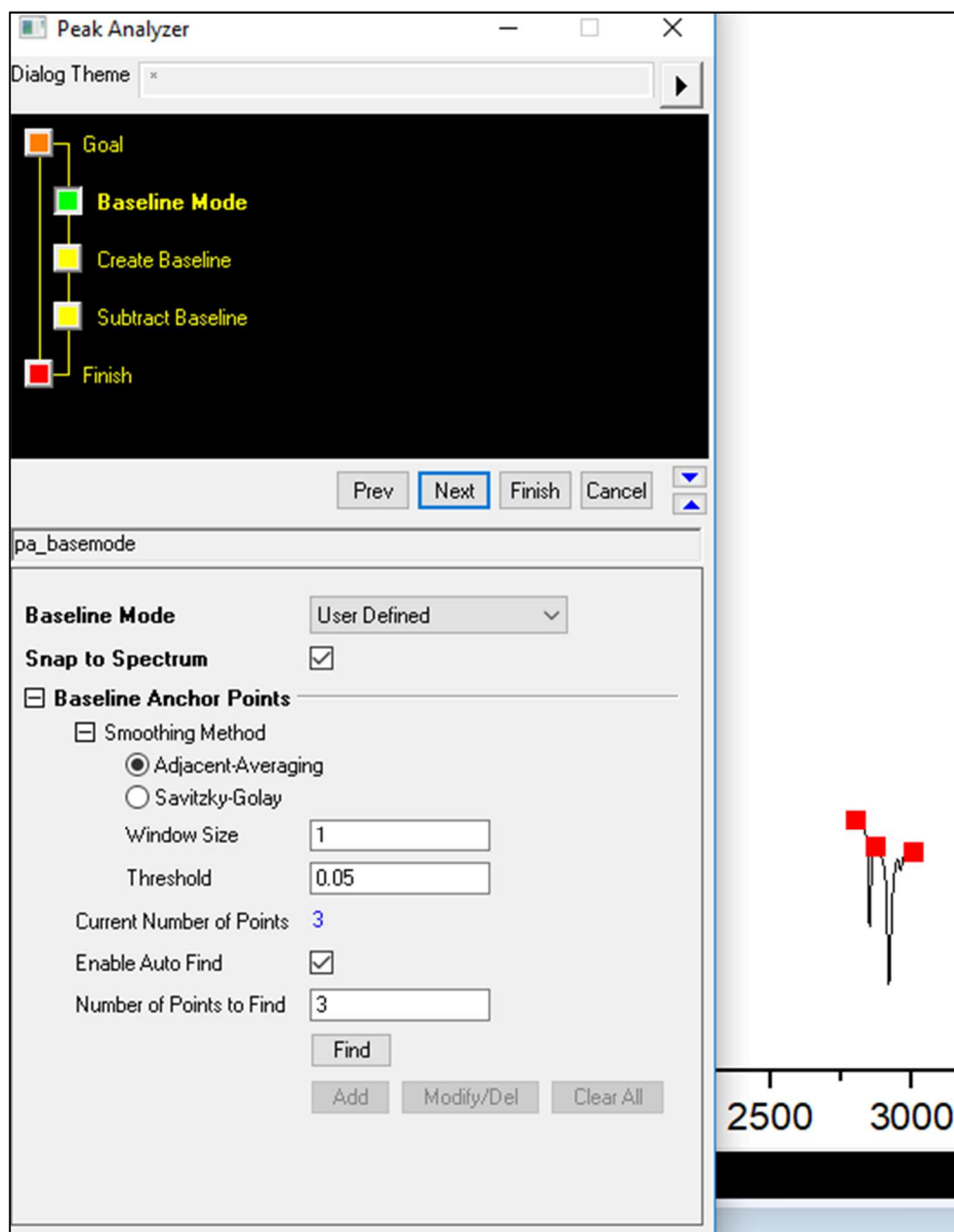
Choosing Connect by interpolation generally works, but using Fitting (pro) gives more control. If you use fitting, be prepared to alter the Number of Baseline Points and Function type to make

sure the baseline function converges. You can assess the suitability of the baseline fit by looking at the temporary graph mentioned earlier.
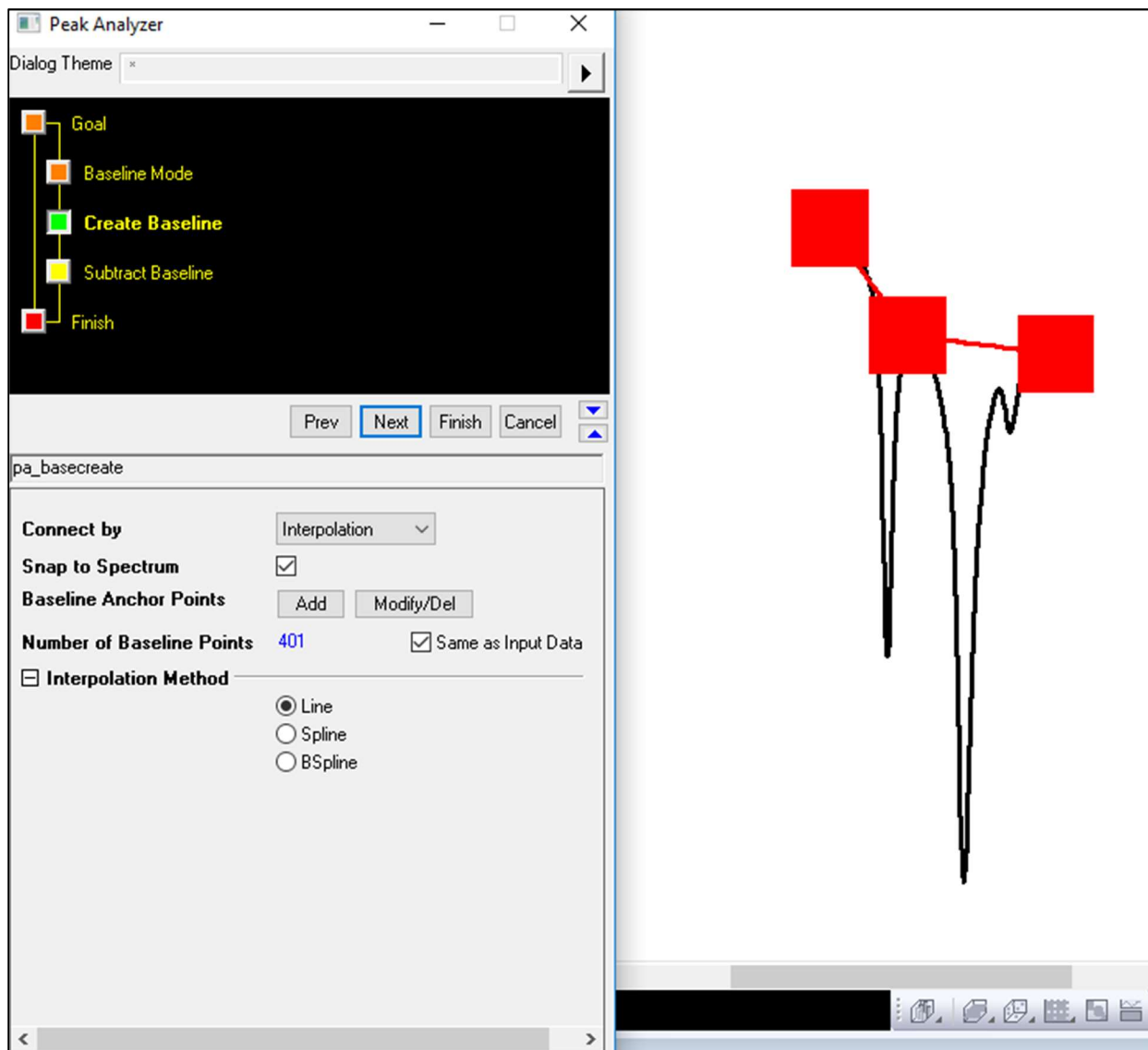
When satisfied, click Next, then specify where you want the subtracted data to be stored. The default is in a new tab within the sheet from which the data came. Click Finish. To plot the subtracted data, choose the "Subtracted" column and plot against your x values. You can then average curves after they have been background subtracted.